



# A highly ordered 8/1 helical pyramidal column self-organized from the crown conformation of achiral hexa(butyloxy)triphenylene

Dipankar Sahoo <sup>a,b</sup>, Emad Aqad <sup>a</sup>, Mihai Peterca <sup>a</sup>, Virgil Percec <sup>a,\*</sup>

<sup>a</sup> Roy & Diana Vagelos Laboratories, Department of Chemistry, University of Pennsylvania, Philadelphia, Pennsylvania, 19104-6323, United States

<sup>b</sup> Department of Medicine, University of Pennsylvania, Philadelphia, Pennsylvania, 19104, United States

**Keywords:** Chiral helical pyramidal columns, Crowns from triphenylene, Nonhelical columns, Discs from triphenylenes, Helical and nonhelical self-organizations, Crystals and liquid crystals

Liquid crystals of disc-like molecules are known for 45 years. 2,3,6,7,10,11-Hexakis(alkyloxy)triphenylene (**HAT $n$** ) containing  $n = 4$  to 11 carbons in its achiral alkyl groups, represents one of the classic families of disc-like molecules. X-ray analysis suggested that disc-like molecules stack on top of each other at irregular spacing in columns distributed in the melt of their alkyl groups forming discotic or columnar or discotic nematic liquid crystals. Interest in discotic liquid crystals comes mostly from their conducting and photoconducting properties. While writing a recent perspective on the 45<sup>th</sup> anniversary of discotic liquid crystals we realized that the molecular structures of the 3D crystal and 2D liquid crystal phases of discotic molecules were never determined at the molecular level, in spite of the great interest in their physical properties. Since structure determines function, we decided to perform a detailed investigation of the molecular structure of **HAT $n$**  self-organizations by reconstructing their oriented fiber X-ray diffractograms both in the crystal and liquid crystal states. This communication reports the synthesis, analysis by differential scanning calorimetry of **HAT $n$**  containing  $n = 4$  to 12 carbons in its achiral alkyl groups and the molecular structure of **HAT4** in its crystal and liquid crystal states. Unexpectedly, a highly ordered 8/1 helical pyramidal crystalline column assembled from a crown-like conformation of the **HAT4** and a non-helical column of the discotic liquid crystal state, the last similar to the original suggested supramolecular structure, were resolved for the first time at the molecular level. These preliminary results raise a lot of fundamental issues in the area of discotic and columnar self-organizations and of related helical columnar self-organizations generated with different building blocks and belonging to different disciplines. A comprehensive mechanistic elucidation of the molecular details of helical and non-helical self-organizations in synthetic complex systems may become as influential in the field of soft condensed matter as that of helical and non-helical self-organizations in the field of molecular biology.

## Introduction

Most probably, the first examples of columnar lyotropic liquid crystals were the water solutions of Tobacco Mosaic Virus (TMV) reported by Bawden, Pirie, Bernal, and Fankuchen in 1936 [1] and continued by the same laboratory in 1937 [2] and in 1941 [3,4].

\* Corresponding authors.

E-mail address: [percec@sas.upenn.edu](mailto:percec@sas.upenn.edu) (V. Percec).

Received 23 November 2022; Received in revised form 6 December 2022; Accepted 8 December 2022

The molecular structure of TMV was elucidated by Rosalind Franklin [5] and Aaron Klug [6] laboratories. A. Klug received Nobel Prize in Chemistry in 1982 for elucidating the structure of biological assemblies while Rosalind Franklin passed away of cancer in 1958. TMV, a helical co-assembly of proteins with RNA, followed the simpler columnar assemblies of the  $\alpha$ -helical proteins and the double helix of nucleic acids that pioneered the field of molecular biology [7,8]. The discovery of helical synthetic macromolecules was briefly discussed by one of us [9] and it will not be repeated here. However, we must mention that the most influential synthetic helical macromolecule that influenced the field of supramolecular chemistry by bridging between macromolecular and supramolecular chemistry to generate the bioinspired synthesis of complex systems is based on the *cis*-stereoisomers of poly(phenyl acetylene) discovered by one of us [10–15]. Discotic liquid crystals were the next molecules that impacted the field of helical assemblies [16–17]. The first helical columnar structure was reported in hexakis(hexylthio)triphenylene [18,19], being of great interest due to its high charge carrier mobility [20]. However, the molecular structure of helical hexakis(hexylthio)triphenylene was never determined at the molecular level. Substantial effort was dedicated to the study of discotic 2,3,6,7,10,11-hexakis(alkyloxy)triphenylene (**HATn**) and of many other discotic molecules. However, the self-organized structure of the most fundamental **HATn** assemblies were never determined at the molecular level [21–27]. The hexaalkyloxy-substituted crown conformation of cyclotrimeratrylene (CTV) was claimed to display pyramidal columnar mesophases [28–32]. Although X-ray studies were performed on CTV assemblies no molecular structure of their self-organizations were determined [33]. Helical columnar assemblies were reported for libraries of self-assembling dendrons [34–57] and self-organizable dendronized polymers [57–82].

## Methods

### Materials

1,2-Dimethoxybenzene (99.0+%), *n*-alkyl bromides, DMF, dichloromethane, acetic acid, hydrobromic acid anhydrous  $K_2CO_3$ , sulfuric acid,  $FeCl_3$  (all from Fisher, ACS reagents) were used as received. Silica gel (60 Å, 32–63  $\mu$ m) was purchased from Sorbent Technology. Dichloromethane (Fisher, ACS reagent grade) was refluxed over  $CaH_2$  and freshly distilled before use. All other chemicals were commercially available and were used as received.

### Techniques

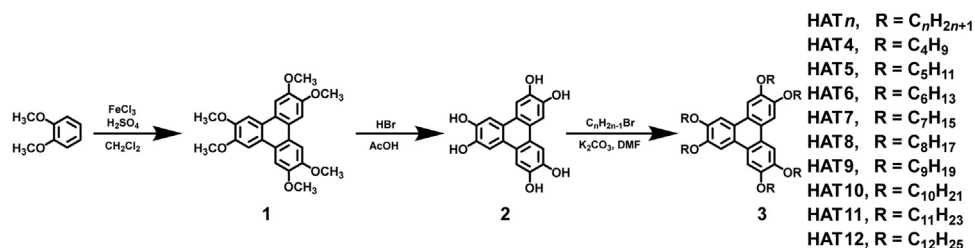
**Nuclear magnetic resonance (NMR) spectroscopy.**  $^1H$  NMR (500 MHz) and  $^{13}C$  NMR (126 MHz) spectra were recorded on a Bruker DRX 500 instrument at 300K or other temperature indicated. Chemical shifts ( $\delta$ ) are reported in ppm and agree with literature data [85]. Coupling constants ( $J$ ) in Hertz (Hz) are therefore, not reported. The resonance multiplicities in the  $^1H$  NMR spectra are described as “s” (singlet), “d” (doublet), “t” (triplet), “quint” (quintet) and “m” (multiplet) and broad resonances are indicated by “br”. Residual protic solvent of  $CDCl_3$  ( $^1H$ ,  $\delta$  7.26 ppm;  $^{13}C$ ,  $\delta$  77.23 ppm, middle of the triplet), and tetramethylsilane (TMS,  $\delta$  0 ppm) were also used as the internal reference in the  $^1H$  and  $^{13}C$  spectra.

**Matrix-assisted laser desorption/ionization time-of-flight (MALDI-TOF).** Matrix-assisted laser desorption/ionization time-of-flight (MALDI-TOF) mass spectrometry was performed on a PerSeptive Biosystems-Voyager-DE (Framingham, MA) mass spectrometer equipped with a nitrogen laser (337  $\mu$ m) and operating in linear mode. Internal calibration was performed using Angiotensin II and Bombesin as standards. The analytical sample was obtained by mixing the THF solution of the sample (5–10mg/ml) and THF solution of the matrix (3,5-dimethoxy-4-hydroxy-*trans*-cinnamic acid or 4-hydroxybenzylidenemalononitrile, 10mg/mL) in a 1/5 v/v ratio. The prepared solution of the sample and the matrix (0.5  $\mu$ L) was loaded on the MALDI plate and allowed to dry at 23°C before the plate was inserted into the vacuum chamber of the MALDI instrument. The laser steps and voltages applied were adjusted depending on both the molecular weight and the nature of each analyzed compound. All MALDI-TOF data agree with the theoretical values. They are confirming the structure of all compounds and therefore, are not reported.

**Thin-layer chromatography (TLC) and high-pressure liquid chromatography (HPLC).** The purity of the products was determined by a combination of thin-layer chromatography (TLC) on silica gel coated aluminum plates (with  $F_{254}$  indicator; layer thickness, 200  $\mu$ m; particle size, 2–25  $\mu$ m; pore size 60Å, SIGMA-Aldrich), high pressure liquid chromatography (HPLC),  $^1H$ -NMR spectroscopy and matrix-assisted laser desorption/ionization time-of-flight (MALDI-TOF) mass spectrometry. HPLC experiments were performed with THF as mobile phase at 1 mL/min, on a Shimadzu LC-10AT high pressure liquid chromatograph equipped with a Perkin Elmer LC-100 oven (40°C), containing two Perkin-Elmer PL gel columns of  $5 \times 10^2$  and  $1 \times 10^4$  Å, a Shimadzu SPD-10A UV detector ( $\lambda = 254$  nm), a Shimadzu RID-10A RI-detector, and a PE Nelson Analytical 900 Series integrator data station.

**Differential scanning calorimetry (DSC).** Thermal transitions were determined with a TA Instruments Q100 differential scanning calorimeter (DSC) equipped with a refrigerated cooling system with  $10^{\circ}C$   $min^{-1}$  heating and cooling rates. Indium was used as calibration standard. The transition temperatures were calculated as the maxima and minima of their endothermic and exothermic peaks. An Olympus BX51 optical microscope (100 X magnifications) equipped with a Mettler FP82HT hot stage and a Mettler Toledo FP90 Central Processor was used to verify thermal transitions and to characterize anisotropic textures. Melting points were measured using a uni-melt capillary melting point apparatus (Arthur H. Thomas Company) and were uncorrected. Density ( $\rho_{20}$ ) measurements were carried out by flotation in gradient columns at 20°C.

**Density Measurements.** For density measurements, a small mass of sample ( $\sim 0.4$  mg) was placed in a vial filled with water followed by ultrasonication to remove the air bubbles embedded within the sample. The sample sank to the bottom of the vial due to its high density compared with water. A saturated aqueous solution of potassium iodide (KI) was then added into the solution at  $\sim 0.1$  g per aliquot to gradually increase the solution density. KI was added

**Fig. 1**

Synthesis of hexakis(alkyloxy)triphenylenes **HATn** with  $n = 4-12$ .

at an interval of at least 20 min to ensure equilibrium within the solution. When the sample was suspended in the middle of the solution, the density of the sample was identical to that of the solution, which was measured by a 10 mL volumetric flask.

**Preparation of oriented fibers for X-ray analysis.** Aligned samples for fiber XRD experiments were prepared using a custom-made extrusion device [83]. The powdered sample ( $\sim 10$  mg) was heated inside the extrusion device above isotropization temperature. After slow cooling from the isotropic phase, the fiber was extruded in the liquid crystal phase and cooled to 23°C. Typically, the aligned samples have a thickness of  $\sim 0.3-0.7$  mm and a length of  $\sim 3-7$  mm. All XRD measurements were done with the aligned sample axis perpendicular to the beam direction.

**X-ray diffraction (XRD).** X-ray diffraction (XRD) measurements were performed using Cu-K $\alpha$ 1 radiation ( $\lambda = 1.54178$  Å) from a Bruker-Nonius FR-591 rotating anode X-ray source equipped with a  $0.2 \times 0.2$  mm $^2$  filament operated at 3.4 kW. The Cu radiation beam was collimated and focused by a single bent mirror and sagitally focused through a Si (111) monochromator, generating in a  $0.3 \times 0.4$  mm $^2$  spot on a Bruker-AXS Hi-Star multiwire area detector. To minimize attenuation and background scattering, an integral vacuum was maintained along the length of the flight tube and within the sample chamber. Samples were held in quartz capillaries (0.7 – 1.0 mm in diameter), mounted in a temperature-controlled oven (temperature precision:  $\pm 0.1$ °C, temperature range from  $-120$ °C to  $270$ °C). The distance between the sample and the detector was 9.0 cm for wide angles diffraction experiments. XRD peaks position and intensity analysis was performed using Datasqueeze Software (version 3.0.8) [84] that allows background elimination and Gaussian, Lorentzian, Lorentzian squared, or Voigt peak-shape fitting was used for X-ray analysis.

### Synthesis

The synthesis of hexakis(alkyloxy)triphenylenes **HATn** with  $n = 4-12$  is outlined in **Fig. 1**. Hexakis(methoxy)triphenylene **1** was synthesized by following modified literature procedures for the trimerization of veratrole catalyzed by FeCl<sub>3</sub> in CH<sub>2</sub>Cl<sub>2</sub> in the presence of a catalytic amount of H<sub>2</sub>SO<sub>4</sub> [53,85–88]. Complete demethylation of hexakis(methoxy)triphenylene using concentrated aqueous HBr in refluxing acetic acid produced hexahydroxytriphenylene **2** [53,87]. Subsequent alkylation of **2**

with linear *n*-alkyl bromide derivatives having 4 to 12 carbon atoms produced **HATn** ( $n = 4-12$ ) respectively.

### General procedure for the *o*-alkylation of 2,3,6,7,10,11-hexahydroxytriphenylene (2)

Dry DMF (10 mL for 1 mmol of 2,3,6,7,10,11-hexahydroxytriphenylene **2**) and finely grinded dry K<sub>2</sub>CO<sub>3</sub> (1.5 equivalents for each hydroxyl group of **2**) were charged in a three-neck round bottom flask equipped with a condenser and magnetic stirring bar. The K<sub>2</sub>CO<sub>3</sub> suspension was degassed at 50°C for 0.5 h under efficient stirring. When the degassing was completed, compound **2** was added while purging the system with Ar. After the complete dissolution of **2**, the *n*-alkyl bromide derivative (7 equivalents for each equivalent of the hexahydroxytriphenylene **2**), was added to the reaction mixture and the temperature was raised to 75°C. The suspension was stirred at 75°C under Ar until the reaction was completed (thin layer chromatography (TLC) control, MeOH/CH<sub>2</sub>Cl<sub>2</sub> 1/9 v/v or acetone/hexane 3/7 v/v). The reaction mixture was poured into cold water (10 times the volume of DMF) and stirred for 5 min. The resulting precipitate was filtered, washed with water and dried. The crude product was dissolved in minimum amount of CH<sub>2</sub>Cl<sub>2</sub> and passed through a short pad of silica-gel using CH<sub>2</sub>Cl<sub>2</sub> as an eluent. The CH<sub>2</sub>Cl<sub>2</sub> was removed completely under reduced pressure. The resulting product was further recrystallized from CH<sub>2</sub>Cl<sub>2</sub>/MeOH 1/2 (V/V), filtered and dried. Analytical data including NMR, HPLC, MALDI-TOF and thermal transitions agree with the theoretical values and literature data [88].

**HAT4:** Yield: 86%. <sup>1</sup>H NMR (CDCl<sub>3</sub>,  $\delta$ , ppm, TMS): 1.07 (t, 18H, 6CH<sub>3</sub>(CH<sub>2</sub>)<sub>3</sub>); 1.59 (m, 12H, CH<sub>3</sub>CH<sub>2</sub>CH<sub>2</sub>CH<sub>3</sub>), 1.96 (m, 12H, CH<sub>3</sub>CH<sub>2</sub>CH<sub>2</sub>CH<sub>2</sub>), 4.27 (t, 12H, CH<sub>3</sub>CH<sub>2</sub>CH<sub>2</sub>CH<sub>2</sub>OAr), 7.86 (s, 6H, ArH).

**HAT5:** Yield: 84%. <sup>1</sup>H NMR (CDCl<sub>3</sub>,  $\delta$ , ppm, TMS): 1.01 (t, 18H, 6CH<sub>3</sub>(CH<sub>2</sub>)<sub>4</sub>); 1.47 (m, 12H, CH<sub>3</sub>CH<sub>2</sub>(CH<sub>2</sub>)<sub>2</sub>CH<sub>2</sub>), 1.58 (m, 12H, CH<sub>3</sub>CH<sub>2</sub>CH<sub>2</sub>(CH<sub>2</sub>)<sub>2</sub>), 1.98 (m, 12H, CH<sub>3</sub>(CH<sub>2</sub>)<sub>2</sub>CH<sub>2</sub>CH<sub>2</sub>), 4.26 (t, 12H, CH<sub>3</sub>(CH<sub>2</sub>)<sub>3</sub>CH<sub>2</sub>OAr), 7.87 (s, 6H, ArH).

**HAT6:** Yield: 85%. <sup>1</sup>H NMR (CDCl<sub>3</sub>,  $\delta$ , ppm, TMS): 0.93 (t, 18H, 6CH<sub>3</sub>(CH<sub>2</sub>)<sub>5</sub>); 1.40 (m, 24H, CH<sub>3</sub>(CH<sub>2</sub>)<sub>2</sub>(CH<sub>2</sub>)<sub>2</sub>CH<sub>2</sub>), 1.56 (m, 12H, CH<sub>3</sub>(CH<sub>2</sub>)<sub>2</sub>CH<sub>2</sub>(CH<sub>2</sub>)<sub>2</sub>), 1.93 (m, 12H, CH<sub>3</sub>(CH<sub>2</sub>)<sub>3</sub>CH<sub>2</sub>CH<sub>2</sub>), 4.22 (t, 12H, CH<sub>3</sub>(CH<sub>2</sub>)<sub>4</sub>CH<sub>2</sub>OAr), 7.80 (s, 6H, ArH).

**HAT7:** Yield: 86% <sup>1</sup>H NMR (CDCl<sub>3</sub>,  $\delta$ , ppm, TMS): 0.92 (t, 18H, 6CH<sub>3</sub>(CH<sub>2</sub>)<sub>6</sub>); 1.38 (m, 24H, CH<sub>3</sub>(CH<sub>2</sub>)<sub>2</sub>(CH<sub>2</sub>)<sub>3</sub>CH<sub>2</sub>), 1.55 (m, 24H,

$\text{CH}_3(\text{CH}_2)_2(\text{CH}_2)_2(\text{CH}_2)_2$ , 1.91 (m, 12H,  $\text{CH}_3(\text{CH}_2)_4\text{CH}_2\text{CH}_2$ ), 4.23 (t, 12H,  $\text{CH}_3(\text{CH}_2)_5\text{CH}_2\text{OAr}$ ), 7.82 (s, 6H, ArH).

**HAT8:** Yield: 89%.  $^1\text{H}$  NMR ( $\text{CDCl}_3$ ,  $\delta$ , ppm, TMS): 0.91 (t, 18H,  $6\text{CH}_3(\text{CH}_2)_7$ ); 1.33-1.40 (m, 48H,  $\text{CH}_3(\text{CH}_2)_4(\text{CH}_2)_2\text{CH}_2$ ), 1.56 (m, 12H,  $\text{CH}_3(\text{CH}_2)_4\text{CH}_2(\text{CH}_2)_2$ ), 1.98 (m, 12H,  $\text{CH}_3(\text{CH}_2)_5\text{CH}_2\text{CH}_2$ ), 4.25 (t, 12H,  $\text{CH}_3(\text{CH}_2)_6\text{CH}_2\text{OAr}$ ), 7.80 (s, 6H, ArH).

**HAT9:** Yield: 89%.  $^1\text{H}$  NMR ( $\text{CDCl}_3$ ,  $\delta$ , ppm, TMS): 0.91 (t, 18H,  $6\text{CH}_3(\text{CH}_2)_8$ ); 1.32-1.37 (m, 60H,  $\text{CH}_3(\text{CH}_2)_5(\text{CH}_2)_2\text{CH}_2$ ), 1.59 (m, 12H,  $\text{CH}_3(\text{CH}_2)_5\text{CH}_2(\text{CH}_2)_2$ ), 1.97 (m, 12H,  $\text{CH}_3(\text{CH}_2)_6\text{CH}_2\text{CH}_2$ ), 4.26 (t, 12H,  $\text{CH}_3(\text{CH}_2)_7\text{CH}_2\text{OAr}$ ), 7.87 (s, 6H, ArH).

**HAT10:** Yield: 94%.  $^1\text{H}$  NMR ( $\text{CDCl}_3$ ,  $\delta$ , ppm, TMS): 0.88 (t, 18H,  $6\text{CH}_3(\text{CH}_2)_9$ ); 1.29-1.43 (m, 72H,  $\text{CH}_3(\text{CH}_2)_6(\text{CH}_2)_2\text{CH}_2$ ), 1.55 (m, 12H,  $\text{CH}_3(\text{CH}_2)_6\text{CH}_2(\text{CH}_2)_2$ ), 1.93 (m, 12H,  $\text{CH}_3(\text{CH}_2)_7\text{CH}_2\text{CH}_2$ ), 4.22 (t, 12H,  $\text{CH}_3(\text{CH}_2)_8\text{CH}_2\text{OAr}$ ), 7.83 (s, 6H, ArH).

**HAT11:** Yield: 92%.  $^1\text{H}$  NMR ( $\text{CDCl}_3$ ,  $\delta$ , ppm, TMS): 0.87 (t, 18H,  $6\text{CH}_3(\text{CH}_2)_{10}$ ); 1.26-1.43 (m, 84H,  $\text{CH}_3(\text{CH}_2)_7(\text{CH}_2)_2\text{CH}_2$ ), 1.55 (m, 12H,  $\text{CH}_3(\text{CH}_2)_7\text{CH}_2(\text{CH}_2)_2$ ), 1.94 (m, 12H,  $\text{CH}_3(\text{CH}_2)_8\text{CH}_2\text{CH}_2$ ), 4.22 (t, 12H,  $\text{CH}_3(\text{CH}_2)_9\text{CH}_2\text{OAr}$ ), 7.83 (s, 6H, ArH).

**HAT12:** Yield: 89%.  $^1\text{H}$  NMR ( $\text{CDCl}_3$ ,  $\delta$ , ppm, TMS): 0.87 (t, 18H,  $6\text{CH}_3(\text{CH}_2)_{11}$ ); 1.26-1.43 (m, 96H,  $\text{CH}_3(\text{CH}_2)_8(\text{CH}_2)_2\text{CH}_2$ ), 1.55 (m, 12H,  $\text{CH}_3(\text{CH}_2)_8\text{CH}_2(\text{CH}_2)_2$ ), 1.94 (m, 12H,  $\text{CH}_3(\text{CH}_2)_9\text{CH}_2\text{CH}_2$ ), 4.22 (t, 12H,  $\text{CH}_3(\text{CH}_2)_{10}\text{CH}_2\text{OAr}$ ), 7.83 (s, 6H, ArH).

### Molecular Modelling and Simulation

Molecular modeling and simulation experiments were performed using Material Studio Modeling (version 3.1) software from Accelrys. Package's Discover module was used to perform the energy minimizations on the supramolecular structures. Details of the methodology for the reconstruction of different helical assemblies are available in different publications [44]. Molecular models of the supramolecular columns were build to match the experimental density of the periodic array and the dimensions of the supramolecular columns. For the construction of the molecular model of the supramolecular column of **HAT4** in the  $\Phi_{\text{r-c}}^{\text{k}}$  phase, first, a single **HAT4** molecule was drawn on DS ViewerPro (5.0). The  $-\text{C}_4\text{H}_9$  chains were attached to the triphenylene center in such a way that they match the column diameter of 17.5 Å (calculated from the XRD data analysis, Table 2) and the tilt angle (25°). The energy minimization of the drawn molecule was performed using Material Studio Modeling software and a **HAT4** molecule with distorted alkyl groups was obtained. Then alkyl groups were again adjusted in such a way that it agrees with the column diameter and tilt angle. Again, the energy optimization was performed on Material Studio Software. The same process was repeated several times until we obtained a molecular model matching the experimental column diameter and tilt angle. Once we obtain a good single molecule with the required column diameter and titling angle with minimized energy, the molecule was employed to build a column of the  $\Phi_{\text{r-c}}^{\text{k}}$  phase. DS ViewerPro software was used to build the column. For  $\Phi_{\text{r-c}}^{\text{k}}$  phase, the molecule takes a crown shape shown in Fig 4e. In the second step, another molecule was placed at a distance of 4.1125 (Å) as it was calculated from the  $c$  parameter (32.9/8 Å) of the 8/1 helical column and the molecule was rotated with an angle

of 45° (360°/8). In this way, the molecules will sit one on top of each other and will form a column. Eight molecules will form a repeat unit in a column of the unit cell in 32.9 Å. Then a crystal lattice was built using the lattice parameter of the  $\Phi_{\text{r-c}}^{\text{k}}$  phase ( $a = 29.0$  Å,  $b = 19.5$  Å, and  $c = 32.9$  Å). The molecular simulation was performed using the obtained crystal in cerius2 software on a silicon graphics computer. Various space groups were used for the  $\Phi_{\text{r-c}}^{\text{k}}$  lattice, and ultimately a very good simulated pattern of the original X-ray diffractogram was obtained using the  $P_{2}1_2_1_2_1$  space group. For the construction of the molecular model of **HAT4** assembly from the  $\Phi_{\text{h}}$  phase, a similar process to be discussed later was employed.

### Results and discussion

The structures of **HATn**,  $n = 4-12$  and their synthesis are shown in Fig. 1. Details of their synthesis are presented in the experimental part. The supramolecular assemblies of the 2,3,6,7,10,11-hexakis(*n*-alkoxy)triphenylene (**HATn**) ( $n = 4-12$ ) were analyzed, characterized, and determined by a combination of DSC, X-ray diffraction of oriented fiber specimens and simulation of the experimental X-ray diffractograms with molecular models constructed as it will be reported later.

The thermotropic phases of the **HATn** series were first identified by the DSC traces collected upon heating and cooling at 10°C/min rate (Fig. 2). They are summarized in Table 1. XRD patterns were collected on oriented fibers at the same heating and cooling rates as the DSC experiments. DSC traces (Fig. 2 and Table 1) indicate that all columnar assemblies of the series of **HATn** exhibit several thermotropic phases before undergoing a transition to the isotropic liquid (**i**). In the case of **HATn** ( $n = 4-10$ ), at low temperatures, center rectangular crystalline phases ( $\Phi_{\text{r-c}}^{\text{k}}$ ) were observed and at higher temperatures, liquid crystalline hexagonal phases ( $\Phi_{\text{h}}$ ) were seen. However, in the case of **HAT11** and **HAT12**, no liquid crystalline phase was observed during heating. In this case we see only the transition from crystalline ( $\Phi_{\text{r-c}}^{\text{k}}$ ) to isotropic phase (**i**).

However, a liquid crystalline hexagonal phase ( $\Phi_{\text{h}}$ ) was detected while cooling as a monotropic phase, in the case of **HAT11**. In the case of **HAT4**, the phase between 76°C and 51°C on cooling is most probably a center rectangular liquid crystalline phase ( $\Phi_{\text{r-c}}$ ) because it has a very small enthalpy change associated with its phase transition, and due to its monotropic character, X-ray analysis is difficult to accomplish at this time.

DSC traces of **HAT4** (Fig. 2, Table 1) indicate that its self-organized structure exhibits two phases before undergoing isotropization at 146 °C. Below 88 °C, there is a crystalline columnar center rectangular phase ( $\Phi_{\text{r-c}}^{\text{k}}$ : **P212121**). From 88 °C to 146 °C, a columnar liquid crystalline hexagonal phase ( $\Phi_{\text{h}}^{\text{IO}}$ : **P6mm**) phase was found. At 146 °C this phase enters the isotropic liquid phase (**i**). The characteristic wide-angle powder X-ray diffraction pattern (WAXS) at 25 °C for **HAT4** is shown in Fig. 4a and its corresponding radial plot at 25 °C is provided in Fig. 4c. The detailed analyses of the X-ray diffractions are shown in Fig. 4a and 4c. These details have also been summarized in Table 2. Fig. 3a shows that there is a discontinuity for the dependence of transition temperatures of **HAT4** to **HAT6** from the same dependence for **HAT6** to **HAT11**.

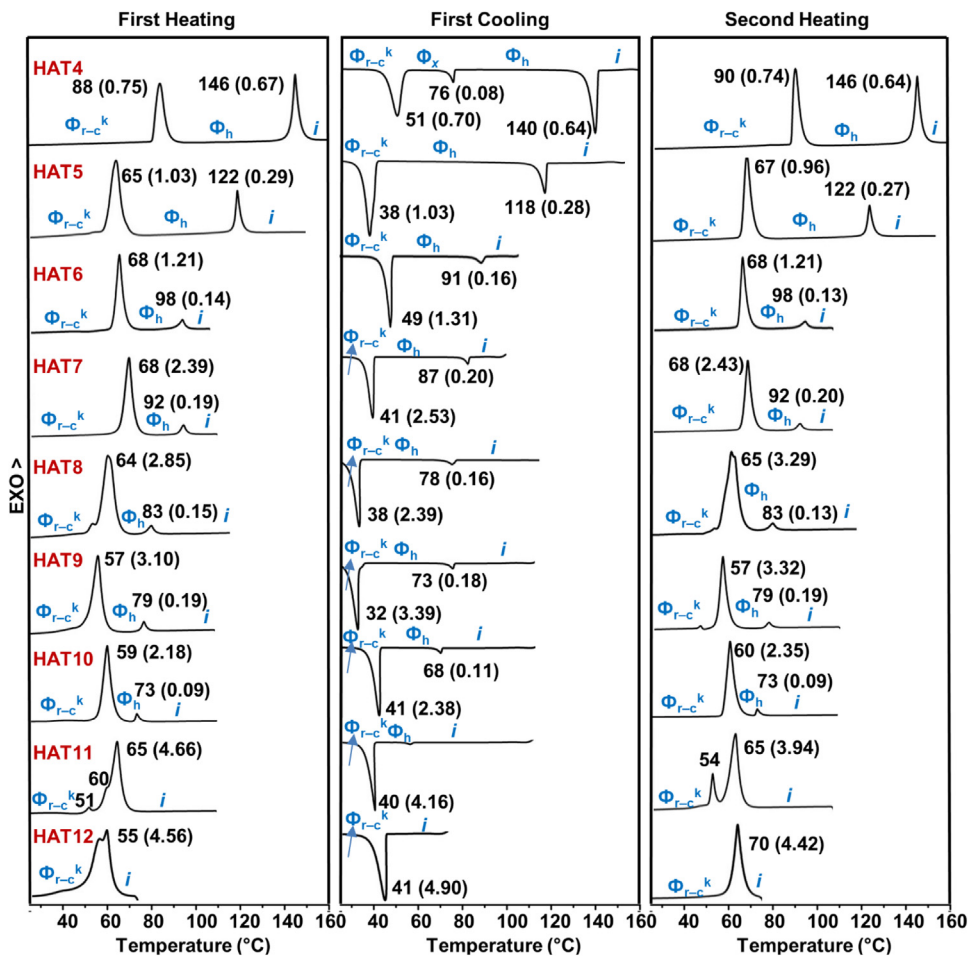


Fig. 2

DSC traces of **HATn** series ( $n = 4–12$ ) recorded with heating and cooling rates of  $10^{\circ}\text{C}/\text{min}$ . Phases determined by XRD, transition temperatures, and associated enthalpy changes (in parentheses in kcal/mol) are indicated. Phase notations:  $\Phi_{r-c}^k$  – Columnar center rectangular crystalline phase;  $\Phi_h$  – Columnar hexagonal liquid crystalline phase;  $\Phi_{r-c}$  – Monotropic columnar center rectangular phase identified by the low enthalpy change of the transition from  $\Phi_h$  phase; the 52 and 60 °C transitions observed on first heating of **HAT11** and the extra peak at 54 °C on the second heat prior the main transition from 65 °C were not identified.

The same kind of discontinuity was previously reported for the dependence of transition temperatures observed at low values of  $n$  for CTTV $n$  reported from two independent laboratories [89,90]. This discontinuity observed both in Fig. 3a and in the CTTV $n$  literature data [89,90] may indicate different mechanisms of self-organization. However, a continuous dependence of transition temperatures was reported for CTV $n$  [29]. This continuous dependence suggests a single mechanism of self-organization for the crown-like conformation of CTV $n$  forming pyramidal columns. The discontinuity of the transition temperatures from Fig. 3a prompted the X-ray analysis experiments reported here for **HAT4**. Fig. 3b plots the dependence of column diameter ( $D_{\text{col}}$ ) for **HATn** with  $n = 4$  to 12 both in the crystal as well as in their liquid crystal self-organizations. Again, a discontinuity was observed in both phases for the **HAT4**, **HAT5** and **HAT6**. In the crystal state a potential odd-even dependence of  $D_{\text{col}}$  vs  $n$  is observed. A similar discontinuity seems to be observed for the liquid crystal state. This discontinuity seems to hold also for the aliphatic width of the columns. However, for the aliphatic region, the discontinuity is not as strong as in the case of  $D_{\text{col}}$  values.

Fig. 3c plots the dependence of the aromatic part area (in % from the top of the entire column area) of the supramolecular columns of **HATn** as a function of  $n$ . Again, a discontinuity of this dependence is observed for the dependence of **HAT4**, **HAT5** and **HAT6** columns vs the columns with larger values of  $n$ . In this plot we see a remarkable difference between the aromatic part area of the columns at  $n = 4, 5$  vs larger values of  $n$ . This indicates that supramolecular columns based on **HAT4** and **HAT5** occupy a much larger fraction of their column by their aromatic part. In fact **HAT4** and **HAT5** columns exhibit an almost identical aromatic area of their columns as the columns self-organized from (3,4,5)dm8\*GI-PBI by the cogwheel mechanism [42]. At higher values of  $n$ , **HATn** self-organizations behave like the CTV $n$  assemblies generated from hat-shaped [41] and other CTV $n$  pyramidal columns. If confirmed by a structural mechanism these results are remarkable for a series of different applications.

The experimental XRD patterns (Fig. 4a) and corresponding radial plot (Fig. 4c) at  $25^{\circ}\text{C}$  indicate that the crystalline phase is a columnar center rectangular crystal phase ( $\Phi_{r-c}^k$ : **P212121**). The measured  $d$ -spacings along the equatorial plane are  $d_{110} = 16.2\text{ \AA}$ ,

Table 1

Thermal analysis of the supramolecular columnar assemblies self-organized from **HAT<sub>n</sub>**, *n* = 4–12

Compound	Phase transition (°C) and corresponding enthalpy changes (kcal·mol <sup>-1</sup> ) <sup>a</sup>	
	Heating	Cooling
<b>HAT4</b>	$\Phi_{r-c}^k$ 88 (0.75) $\Phi_h$ 146 (0.67) <i>i</i> $\Phi_{r-c}^k$ 90 (0.74) $\Phi_h$ 146 (0.64) <i>i</i>	<i>i</i> 140 (-0.64) $\Phi_h$ 76 (-0.08) $\Phi_{r-c}^k$ 51 (-0.70) $\Phi_{r-c}^k$
<b>HAT5</b>	$\Phi_{r-c}^k$ 65 (1.03) $\Phi_h$ 122 (0.29) <i>i</i> $\Phi_{r-c}^k$ 67 (0.96) $\Phi_h$ 122 (0.27) <i>i</i>	<i>i</i> 118 (-0.28) $\Phi_h$ 38 (-1.03) $\Phi_{r-c}^k$
<b>HAT6</b>	$\Phi_{r-c}^k$ 68 (1.21) $\Phi_h$ 98 (0.14) <i>i</i> $\Phi_{r-c}^k$ 68 (1.21) $\Phi_h$ 98 (0.13) <i>i</i>	<i>i</i> 91 (-0.16) $\Phi_h$ 49 (-1.31) $\Phi_{r-c}^k$
<b>HAT7</b>	$\Phi_{r-c}^k$ 68 (2.39) $\Phi_h$ 92 (0.19) <i>i</i> $\Phi_{r-c}^k$ 68 (2.43) $\Phi_h$ 92 (0.20) <i>i</i>	<i>i</i> 87 (-0.20) $\Phi_h$ 41 (-2.53) $\Phi_{r-c}^k$
<b>HAT8</b>	$\Phi_{r-c}^k$ 64 (2.85) $\Phi_h$ 83 (0.15) <i>i</i> $\Phi_{r-c}^k$ 65 (3.29) $\Phi_h$ 83 (0.13) <i>i</i>	<i>i</i> 78 (-0.16) $\Phi_h$ 41 (-2.39) $\Phi_{r-c}^k$
<b>HAT9</b>	$\Phi_{r-c}^k$ 57 (3.10) $\Phi_h$ 79 (0.19) <i>i</i> $\Phi_{r-c}^k$ 57 (3.32) $\Phi_h$ 79 (0.19) <i>i</i>	<i>i</i> 79 (-0.19) $\Phi_h$ 57 (-3.32) $\Phi_{r-c}^k$
<b>HAT10</b>	$\Phi_{r-c}^k$ 59 (2.18) $\Phi_h$ 73 (0.09) <i>i</i> $\Phi_{r-c}^k$ 60 (2.35) $\Phi_h$ 73 (0.09) <i>i</i>	<i>i</i> 68 (-0.11) $\Phi_h$ 41 (-2.38) $\Phi_{r-c}^k$
<b>HAT11</b>	$\Phi_{r-c}^k$ 65 (4.66) <i>i</i> $\Phi_{r-c}^k$ 65 (3.94) <i>i</i>	<i>i</i> 58 (-0.07) $\Phi_h$ 40 (-4.16) $\Phi_{r-c}^k$
<b>HAT12</b>	$\Phi_{r-c}^k$ 55 (4.56) <i>i</i> $\Phi_{r-c}^k$ 70 (4.42) <i>i</i>	<i>i</i> 41 (-4.90) $\Phi_{r-c}^k$

<sup>a</sup> Data from the first heating and cooling scans (at 10°C·min<sup>-1</sup>) are on the first line, and data from the second heating are on the second line;  $\Phi_{r-c}^k$ : **P2<sub>1</sub>2<sub>1</sub>2<sub>1</sub>** crystalline center rectangular columnar phase,  $\Phi_h$ : **P6mm** liquid crystalline hexagonal columnar phase,  $\Phi_{r-c}$  – Columnar center rectangular phase, *i*: isotropic phase.

$d_{200} = 14.5$  Å,  $d_{020} = 9.7$  Å,  $d_{220} = 8.1$  Å,  $d_{130} = 6.3$  Å,  $d_{330} = 5.4$  Å,  $d_{008} = 32.9$  Å (Table 2). The presence of these diffraction spots in the XRD pattern indicates that it is a center rectangular lattice. The lattice parameters at 25 °C are  $a = 29.0$  Å,  $b = 19.5$  Å, and  $c = 33.9$  Å. The presence of intense off-axis diffractions indicates a highly ordered crystalline lattice. The stratum thickness ( $t = 4.1125$  Å) has been calculated from bright intense broad diffraction along the fiber axis ( $d_{008} = 4.1125$  Å) (Fig. 3c). The eight equidistant layer lines,  $L = 0$  to  $L = 8$  from the experimental oriented fiber X-ray diffractogram of Fig. 4a indicate an 8/1 helical column. From the molecular weight of **HAT4**,  $M_{wt} = 660.9$  g·mol<sup>-1</sup>, we determine an average number of molecules,  $\mu$ , forming the supramolecular column stratum with thickness ( $t$ ),  $\mu = N_A At \rho / M_{wt}$  where  $N_A$  (Avogadro's number) =  $6.022 \times 10^{23}$  mol<sup>-1</sup>, where  $A$  is the area of the column cross-section calculated from the lattice parameters,  $\rho$  is the density of the supramolecular structure measured at room temperature (1.02 g/cm<sup>3</sup>) and  $t$  is the stratum thickness. From this calculation, we find that for the  $\Phi_{r-c}^k$  phase, there must be eight molecules per column stratum ( $\mu = 8.3 \sim 8$ ). The approximate column diameter ( $D_{col}$ ) is 17.5 Å (Table 2).

Fig. 4d–h displays the molecular models of the  $\Phi_{r-c}^k$  phase of **HAT4**. The repeat unit is formed by eight molecules (Fig. 4f). In the first step, one molecule is placed with distorted  $-C_4H_9$  alkyl tails (Fig. 4d and 4e). In the second step, another **HAT4** molecule is placed at an average distance of 4.2115 Å but this **HAT4** molecule will be rotated by 45° along the column axis (Fig. 4f). Thus, **HAT4** molecules will sit one on top of another in a similar fashion

(Fig. 4f). In this way, a supramolecular column is formed with an 8/1 helicity (Fig. 4f).

Fig. 4f and Fig. 4g show the side and the top views of the column. Thus, these columns will arrange themselves in a crystalline center rectangular phase ( $\Phi_{r-c}^k$ : **P2<sub>1</sub>2<sub>1</sub>2<sub>1</sub>**) periodic array (Fig. 4h).

Simulation of the X-ray diffractogram was carried out using the molecular models (Fig. 4d–h) and the same cell parameters and **P2<sub>1</sub>2<sub>1</sub>2<sub>1</sub>** space group. The simulated pattern (Fig. 4b) indicates a very good agreement with the experimental XRD patterns (Fig. 4a). The position and melting of the alkyl groups play an important role in the crystal structure. The space group also plays an important role in building the crystals. About fifty molecular models and various space groups of  $\Phi_{r-c}^k$  lattice were used to do the simulation experiment in order to obtain the optimum structure from Fig 4f. The molecular model shown in Fig 4d–h with **P2<sub>1</sub>2<sub>1</sub>2<sub>1</sub>** space group gives a satisfying simulated pattern (Fig. 4b) that is in good agreement with the experimental XRD pattern (Fig. 4a). We would like to mention that the methodology employed to solve the structure of the columnar assembly of **HAT4** relies on the transplant of the Watson and Crick strategy employed to solve the structure of DNA except that in our case both the molecular models and the reconstruction of their oriented fiber X-ray diffractograms were generated by computer software [44,45,50,91].

The experimental XRD pattern at 128 °C in the liquid crystal phase and the corresponding radial plot along the equatorial

Table 2

XRD structural analysis of the columnar assemblies of HAT<sub>n</sub>, n = 4–12

HAT <sub>n</sub> [n = 4–12] <sup>a</sup>	M <sub>wt</sub> (g/mol) <sup>b</sup>	T (°C) <sup>c</sup>	Phase <sup>d</sup>	Lattice Parameters a, b (Å) <sup>e</sup>	D <sub>col</sub> (Å) <sup>f</sup>	D <sub>col</sub> (Å) <sup>g</sup>	μ <sup>h</sup>	d <sub>100</sub> , d <sub>200</sub> , d <sub>020</sub> , d <sub>220</sub> , d <sub>130</sub> , d <sub>310</sub> , d <sub>400</sub> , d <sub>001</sub> , d <sub>005</sub> , d <sub>008</sub> (Å) <sup>i</sup> d <sub>10</sub> , d <sub>11</sub> , d <sub>20</sub> , d <sub>21</sub> (Å) <sup>j</sup>
<b>HAT4</b>	660.9	25	Φ <sub>r-c</sub> <sup>k</sup>	29.0, 19.5	17.5	20.7	8	16.2, 14.5, 9.7, 8.1, 6.3, –, –, –, 4.1 <sup>i</sup>
		128	Φ <sub>h</sub>	18.6, 18.6	18.6	20.7	1	16.2, 9.3, 8.1, 6.2 <sup>j</sup>
<b>HAT5</b>	745.1	25	Φ <sub>r-c</sub> <sup>k</sup>	27.6, 23.6	18.2	17.5	8	18.0, 13.8, 11.8, 8.9, –, 8.6, –, –, 4.1 <sup>i</sup>
		80	Φ <sub>h</sub>	20.8, 20.8	20.8	23.3	1	18.0, –, –, 6.7 <sup>j</sup>
<b>HAT6</b>	829.3	25	Φ <sub>r-c</sub> <sup>k</sup>	36.9, 28.6	18.2	5	22.7, 18.5, 14.3, –, –, 11.3, 9.2, –, 4.2, –	
		70	Φ <sub>h</sub>	21.3, 21.3	21.3	25.9	1	18.5, –, –, – <sup>j</sup>
<b>HAT7</b>	913.4	25	Φ <sub>r-c</sub> <sup>k</sup>	37.0, 31.9	24.4	2	24.2, 18.5, 16.0, 12.1, –, –, 6.1, 4.3, –, – <sup>i</sup>	
		70	Φ <sub>h</sub>	22.7, 22.7	22.7	28.4	1	19.6, 11.4, –, – <sup>j</sup>
<b>HAT8</b>	997.6	25	Φ <sub>r-c</sub> <sup>k</sup>	38.1, 31.0	24.6	2	24.2, 19.1, 15.5, 11.8, –, 12.0, –, 4.3, –, –	
		70	Φ <sub>h</sub>	23.5, 23.5	23.5	31.1	1	20.4, 11.7, –, – <sup>j</sup>
<b>HAT9</b>	1081.7	25	Φ <sub>r-c</sub> <sup>k</sup>	40.2, 37.1	27.3	2	27.5, 20.2, 18.6, 13.6, 10.4, –, –, 4.4, –, –	
		60	Φ <sub>h</sub>	25.1, 25.1	25.1	33.9	1	21.9, 12.5, –, – <sup>j</sup>
<b>HAT10</b>	1165.9	25	Φ <sub>r-c</sub> <sup>k</sup>	46.1, 30.2	31.6	2	25.3, 23.1, 12.7, –, 11.5, –, 9.8, 4.4, –, – <sup>i</sup>	
		60	Φ <sub>h</sub>	26.0, 26.0	26.0	36.5	1	22.4, 13.0, 11.3, – <sup>j</sup>
<b>HAT11</b>	1250.1	25	Φ <sub>r-c</sub> <sup>k</sup>	51.5, 35.2	–	31.2	–	29.1, 25.9, 17.7, 14.6, 11.5, –, –, 4.4, –, – <sup>i</sup>
		60	Φ <sub>h</sub>	26.0, 26.0	–	32.1	–	31.5, 25.3, 20.2, 15.7, 12.9, –, 12.6, 4.4, –, – <sup>i</sup>
<b>HAT12</b>	1334.2	25	Φ <sub>r-c</sub> <sup>k</sup>	50.3, 40.0	–	–	–	–

<sup>a</sup> Name of the HAT<sub>n</sub>, n indicates the alkyl chain length [C<sub>n</sub>H<sub>2n+1</sub>, n = 4–12].<sup>b</sup> Molecular weight of the compound.<sup>c</sup> Temperature in °C.<sup>d</sup> Phase notation: Φ<sub>r-c</sub><sup>k</sup> – Columnar center rectangular crystalline phase; Φ<sub>h</sub> – Columnar hexagonal liquid crystalline phase;<sup>e</sup> Lattice parameters determined from fiber X-ray diffractions; a = h d<sub>100</sub> and b = k d<sub>001</sub> for Φ<sub>r-c</sub><sup>k</sup> phase; a = (2/√3)(d<sub>10</sub> + √3d<sub>11</sub> + 2d<sub>20</sub>)/3 for Φ<sub>h</sub> phase.<sup>f</sup> Column diameter (experimental) for Φ<sub>r-c</sub><sup>k</sup> phase calculated using D<sub>col</sub> = a/[2cos(tan<sup>-1</sup>b/a)]. Column diameter (experimental) for Φ<sub>h</sub> phase calculated using D<sub>col</sub> = a.<sup>g</sup> Diameter of the columns with alkyl trails extended and straight.<sup>h</sup> Number of dendrons per column stratum calculated from  $\mu = VN_A t \rho / M_{wt}$ , where V = unit cell volume, N<sub>A</sub> = Avogadro number, t = column stratum average thickness, ρ = the density of the supramolecular structure measured at room temperature, M<sub>wt</sub> = molecular weight, estimated error  $\Delta\mu = \pm 10\%$ .<sup>i</sup> Experimentally derived d-spacings for the Φ<sub>r-c</sub><sup>k</sup> phase  $d_{hkl} = [(h/a)^2 + (k/b)^2 + (l/c)^2]^{-1/2}$  for center rectangular lattices.<sup>j</sup> Experimentally derived d-spacings for the Φ<sub>h</sub> phases calculated using:  $d_{hkl} = [4(h^2 + k^2 + hk)/(3a^2) + (l/c)^2]^{-1/2}$ .<sup>5</sup> Fiber direction.

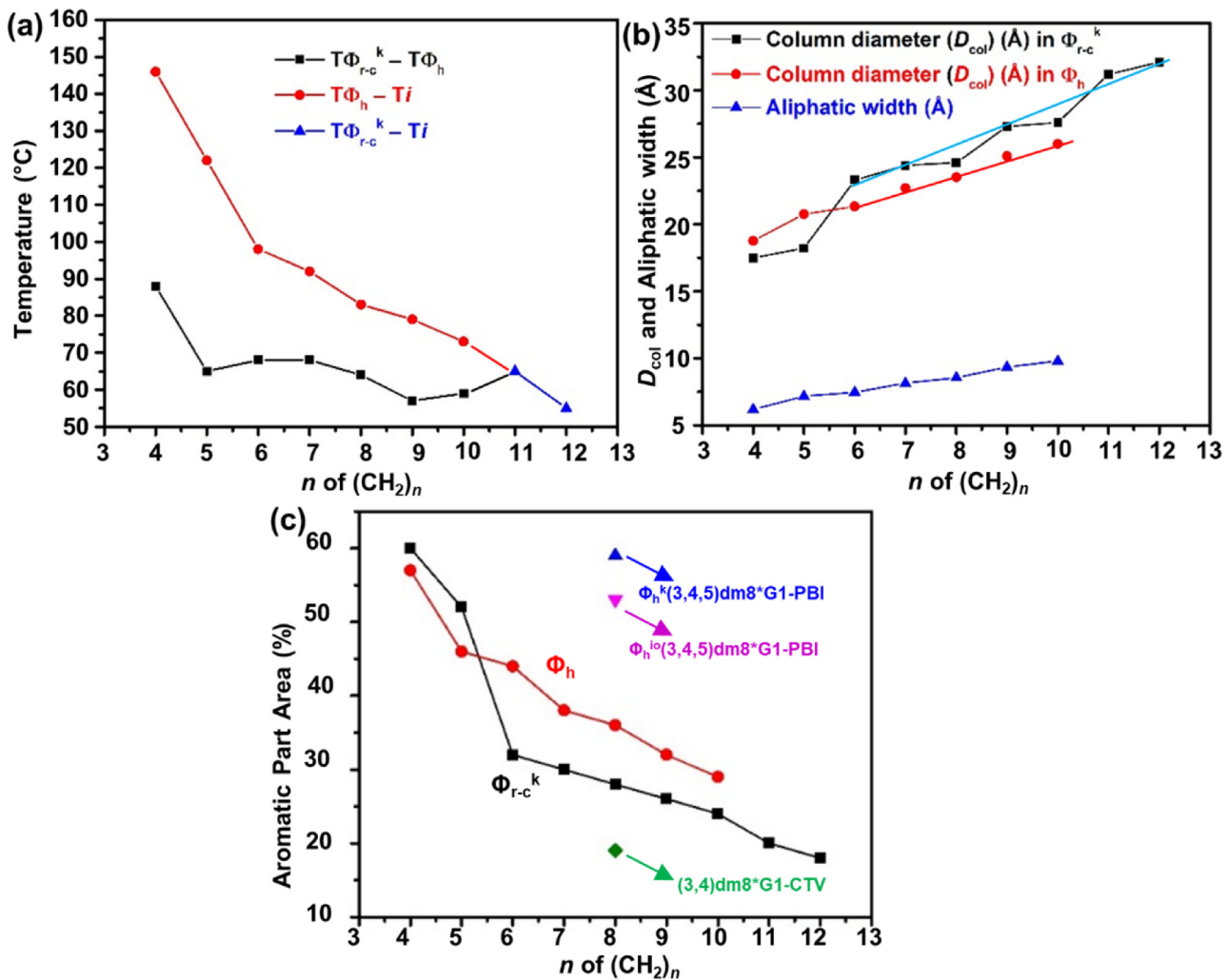


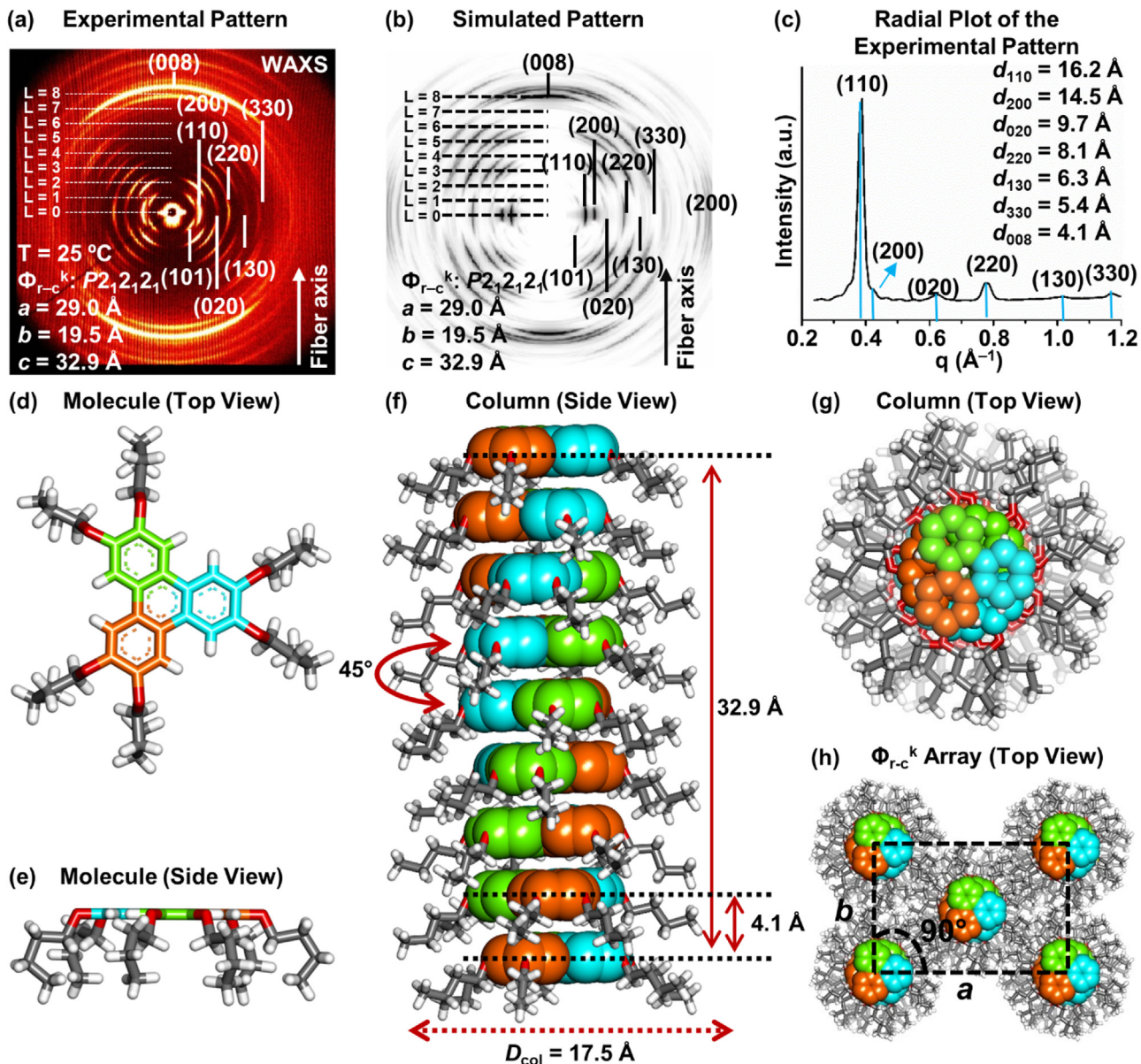
Fig. 3

(a) Temperature transitions vs  $n$  of **HATn**, (b) Dimensions of columns diameter in crystal, liquid crystal and the aliphatic thickness of **HATn** vs  $n$ ; the cyan line is attempting to connect the column diameters in the  $\Phi_{r-c}^k$  phase in a linear way demonstrating a more complex dependence on  $n$ ; (c) The fraction of the aromatic part from the total lattice cross-section in different regions and periodic arrays of the column (%) vs  $n$  of **HATn** are compared with the same data for the cogwheel mechanism ((3,4,5)dm8\*G1-PBI,  $\Phi_h^k$  and  $\Phi_h^{lo}$  lattice) from reference [42] and of the hat-shaped columns (3,4)dm8\*G1-CTV) from reference [41]. The aromatic area was calculated by  $(\Delta A / \Delta V) * 100$ , where  $\Delta A$  is the area of the cross-section occupied by the aromatic part and  $\Delta V$  is the cross-section of the unit cell.

plane are shown in Fig. 5a and 5c. The diffraction spots in the XRD pattern whose reciprocal  $d$ -spacings are in the ratio  $d_{100}:d_{110}:d_{200}:d_{210} = 1:1/\sqrt{3}:1/2:1/\sqrt{7}$  can be indexed as a hexagonal lattice. The measured  $d$ -spacings along the equatorial plane are  $d_{100} = 16.2 \text{ \AA}$ ,  $d_{110} = 9.3 \text{ \AA}$ ,  $d_{200} = 8.1 \text{ \AA}$ ,  $d_{210} = 6.2 \text{ \AA}$ , and  $d_{001} = 3.6 \text{ \AA}$  (Fig. 4a,c and Table 2) and lattice parameters  $a = b = 18.6 \text{ \AA}$ . The absence of any off-axis diffractions indicates that it is a columnar liquid crystalline lattice. The presence of the meridional broad diffraction along the fiber axis (Fig. 4a) ( $d_{001} = 3.6 \text{ \AA}$ ) indicates the stratum distance ( $t = 3.6 \text{ \AA}$ ). Absence of any off-axis diffraction indicates a non-helical column. We calculate an average number of molecules forming the supramolecular column stratum with thickness ( $t$ ) using the formula  $\mu = N_A A t \rho / M_{\text{wt}}$ , where  $N_A$  (Avogadro's number) =  $6.022 \times 10^{23} \text{ mol}^{-1}$ , where  $A$  is the area of the column cross-section calculated from the lattice parameters,  $\rho$  is the density of the compound, measured at room temperature

( $1.02 \text{ g/cm}^3$ ) and  $t$  is the stratum thickness ( $3.6 \text{ \AA}$ ), and  $M_{\text{wt}}$  is molecular weight ( $M_{\text{wt}} = 660.9 \text{ g.mol}^{-1}$ ). From this calculation, we conclude that in the  $\Phi_h$  phase, there is only one molecule per column stratum ( $\mu = 1.1 \sim 1$ ). The column diameter ( $D_{\text{col}}$ ) is  $18.6 \text{ \AA}$  (Table 2).

Fig. 5d-h shows the molecular models for the  $\Phi_h$  phase. There is only one **HAT4** molecule per column stratum of thickness  $3.6 \text{ \AA}$  (Fig. 5f). The **HAT4** molecule is placed with highly distorted, melted, liquid-like  $-\text{C}_4\text{H}_9$  alkyl tails, in the plane of the planar part of **HAT4** as well as some of them up and some down (Fig. 5d and 5e). In the next step, a second **HAT4** molecule is placed at an approximate distance of  $3.6 \text{ \AA}$  (Fig. 5f). Thus, the planar part of **HAT4** molecules will form a column (Fig. 5f and 5g) that is embedded in the melted state of its own alkyl groups. These supramolecular columns will self-organize in a columnar hexagonal liquid crystalline phase ( $\Phi_h$ : **P6mm**) (Fig. 5h). The reconstructed X-ray pattern (Fig. 5b) generated with

**Fig. 4**

X-Ray diffraction analysis and molecular models of **HAT4** at 25°C ( $\Phi_{r-c}^k$  phase). (a) Wide-angle fiber XRD (WAXS) patterns of **HAT4** collected at 25 °C showing the (110), (200), (020), (220), (130), (330), and (008) diffractions indicating a columnar center rectangular phase ( $\Phi_{r-c}^k$ ). The fiber axis is vertical. (b) Simulated XRD patterns from the molecular model. (c) Radial plots; equatorial of the WAXS experimental XRD pattern showing the (110), (200), (020), (220), (130), (330), and (008) diffractions indicating the  $\Phi_{r-c}^k$  phase. (d) Single molecule (Top View). (e) Single molecule (Side View). (f) Formation of the column by stacking of the molecules with a distance of 4.1 Å and 45° rotation along the fiber axis (Side View) showing the helicity (8/1). (g) Formation of the column (Top View) of the  $\Phi_{r-c}^k$  phase. (h) Center rectangular array formed by the columns (Top View). Color code used in the model: O atoms, red; H atoms, white; C atoms in the phenyl rings, orange, green, and blue; all other C atoms, grey. Black dot lines in (h) indicate the lattice parameters.

the molecular models of the  $\Phi_h$  phase (Fig. 5d-h) indicate an excellent agreement with the experimental XRD pattern (Fig. 5a). We would like to mention that this is the first reconstruction of the X-ray pattern of an oriented  $\Phi_h$  phase, demonstrating definitively the model advanced by Chandrasekhar laboratory in 1977 [16,17].

## Conclusions

**HAT4** self-organizes in a highly ordered crystalline 8/1 helical pyramidal column *via* the crown conformation of its disc-like triphenylene molecule. This unexpected mechanism

of self-organization was never reported or even considered for hexakis(alkyloxy)triphenylenes. The mechanism of self-organization shown in Fig. 4 resembles the cogwheel mechanism of dendronized perylenebisimide, PBIs, that was recently discovered in our laboratory [42]. Therefore, the self-organization of **HAT4** is expected to be extraordinarily accelerated, *via* proper molecular design, as it was demonstrated for the cogwheel model of self-organization [92,93]. This discovery is extremely important since helical self-organization of achiral **HATn** was never observed before being reported here. In addition, the

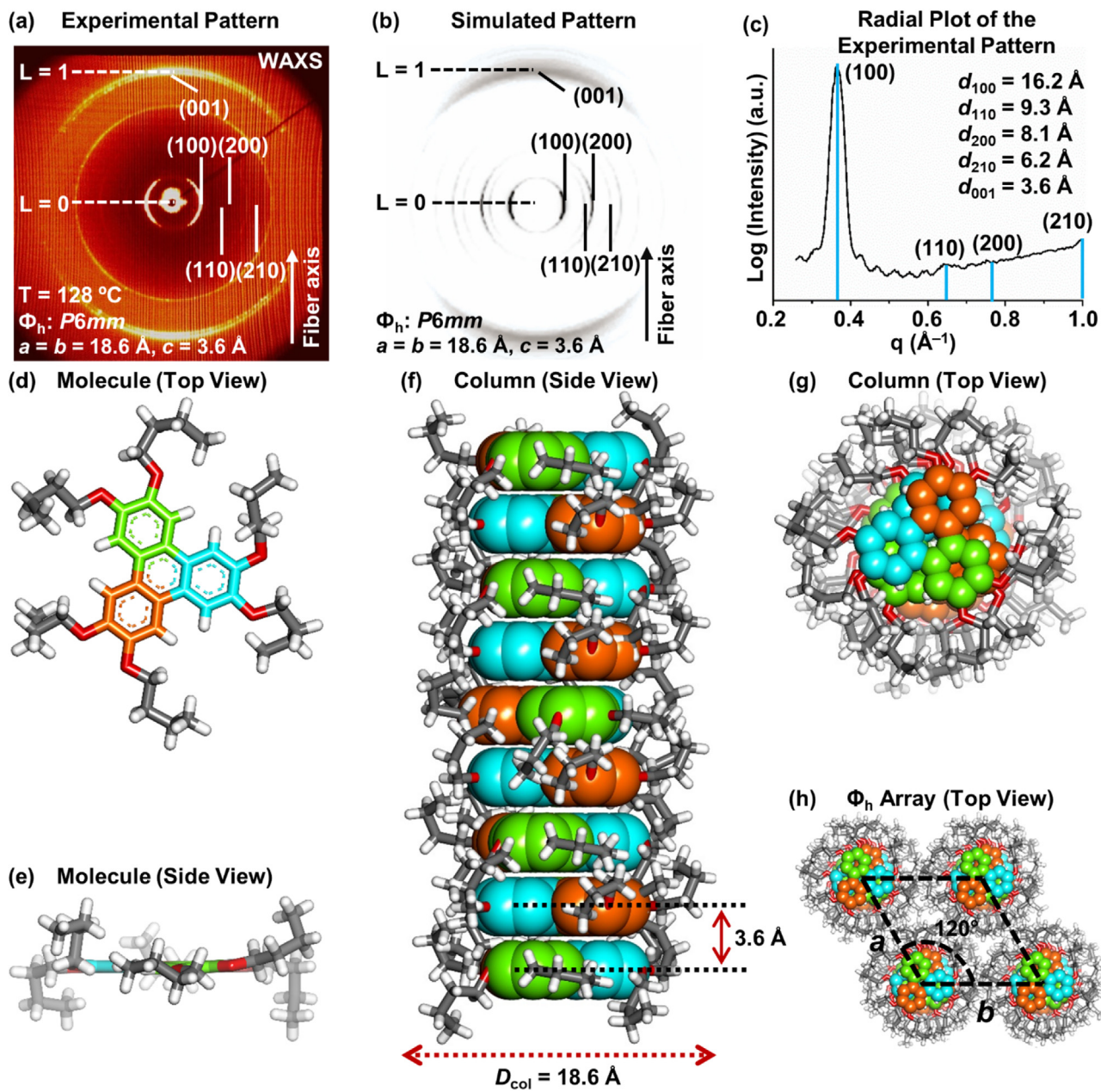


Fig. 5

X-ray diffraction analysis and molecular models of **HAT4** at 128 °C ( $\Phi_h$  phase). (a) Wide-angle fiber XRD (WAXS) patterns of **HAT4** collected at 128 °C showing the (100), (110), (200), and (210) diffractions indicating a columnar hexagonal phase ( $\Phi_h$ ). The fiber axis is vertical. (b) Simulated XRD patterns from the molecular model. (c) Radial plots; equatorial of the WAXS experimental XRD pattern showing the (100), (110), (200), and (210) diffractions indicating the  $\Phi_h$  phase. (d) Single molecule (Top View). (e) Single molecule (Side View). (f) Formation of the column by stacking of the molecules with a distance of 3.6 Å (Side View). (g) Formation of the column (Top View) of the  $\Phi_h$  phase. (h) Hexagonal array formed by the columns (Top View). Color code used in the model: O atoms, red; H atoms, white; C atoms in the phenyl rings, orange, green, and blue; all other C atoms, grey. Black dot lines in (h) indicate the lattice parameters.

large surface area of the triphenylene in this periodic array indicates that cogwheel like self-organizations maybe most interesting for the design of highly efficient complex functional systems based on columnar hexagonal assemblies. Therefore, it is interesting to elucidate the molecular mechanism *via* which the transition from **HAT4** to **HATn** with larger values of *n* occurs. This work is in progress and will contribute to the elucidation of the mechanism and the generality of helical chirality formation in supramolecular and macromolecular

assemblies [41,42,44,45,46,50,53,55,70,72,73,74,76,94,95,96] and to its induction in even more complex systems [97]. It is interesting that the transition from  $\Phi_{r-c}^k$  to  $\Phi_h$  was accompanied by a transition from a helical column to a non-helical column that is not yet elucidated [98,99]. The only other helical self-organization of disc-like triphenylene was reported for hexakis(hexylthio)triphenylene [18,19], but the molecular structure of its supramolecular columns was not determined. Helical triphenylenes self-organized from triphenylene crowns

were also obtained by dendronizing triphenylenes with self-assembling dendrons [53]. Crown self-assembling conformations are responsible for the development of new concepts in helical self-organization [100–105], and we expect that they will play an important role in the development of synthetic self-organizations [106–112] with the dimensions and perfection of complex biological systems [5,6,7,8,9].

## Declaration of Competing Interest

The authors declare that they have no known competing financial interests or personal relationships that could have appeared to influence the work reported in this paper.

## Declaration of competing interest

The authors declare no competing interests in this paper.

## Data Availability

Data will be made available on request.

## Acknowledgment

Financial support by the National Science Foundation (DMR-1807127, DMR-1720530, and DMR- 2104554), the Humboldt Foundation, and the P. Roy Vagelos Chair at Penn (all to V.P.) is gratefully acknowledged.

## References

- [1] F.C. Bawden, N.W. Pirie, J.D. Bernal, I. Fankuchen, Liquid crystalline substances from virus-infected plants, *Nature* 138 (1936) 1051–1052, doi:10.1038/1381051a0.
- [2] J. Bernal, I. Fankuchen, Structure types of protein crystals from virus-infected plants, *Nature* 139 (1937) 923–924, doi:10.1038/139923a0.
- [3] J.D. Bernal, I. Fankuchen, X-ray and crystallographic studies of plant virus preparations: I. Introduction and preparation of specimens II. Modes of aggregation of the virus particles, *J. Gen. Physiol.* 25 (1941) 111–146, doi:10.1085/jgp.25.1.111.
- [4] J.D. Bernal, I. Fankuchen, X-ray and crystallographic studies of plant virus preparations, *J. Gen. Physiol.* 25 (1941) 147–165, doi:10.1085/jgp.25.1.147.
- [5] V. Percec, Q. Xiao, The legacy of Rosalind E. Franklin: Landmark contributions to two Nobel Prizes, *Chem* 7 (2021) 529–536, doi:10.1016/j.chempr.2021.02.020.
- [6] A. Klug, From macromolecules to biological assemblies (Nobel Lecture), *Angew. Chem., Int. Ed. Engl.* 22 (1983) 565–582, doi:10.1002/anie.198305653.
- [7] V. Percec, Q. Xiao, Helical chirality of supramolecular columns and spheres self-organizes complex liquid crystals, crystals, and quasicrystals, *Isr. J. Chem.* 61 (2021) 530–556, doi:10.1002/ijch.202100057.
- [8] V. Percec, Q. Xiao, Helical self-organizations and emerging functions in architectures, biological and synthetic macromolecules, *Bull. Chem. Soc. Jpn.* 94 (2021) 900–928, doi:10.1246/bcsj.20210015.
- [9] V. Percec, Merging macromolecular and supramolecular chemistry into bioinspired synthesis of complex systems, *Isr. J. Chem.* 60 (2020) 48–66, doi:10.1002/ijch.202000004.
- [10] C.I. Simionescu, V. Percec, S. Dumitrescu, Polymerization of acetylenic derivatives. XXX. Isomers of polyphenylacetylene, *J. Polym. Sci. Part A Polym. Chem. Ed.* 15 (1977) 2497–2509, doi:10.1002/pol.1977.170151018.
- [11] C.I. Simionescu, V. Percec, Thermal cis-trans isomerization of cis-transoidal polyphenylacetylene, *J. Polym. Sci. Part A Polym. Chem.* 18 (1980) 147–155, doi:10.1002/pol.1980.170180114.
- [12] C.I. Simionescu, V. Percec, Polypentadeuterophenylacetylene isomers, *J. Polym. Sci. Part C Polym. Lett.* 17 (1979) 421–429, doi:10.1002/pol.1979.130170705.
- [13] C.I. Simionescu, V. Percec, Polyarylacetylenes: structure and properties, *J. Polym. Sci. Polym. Symp.* 67 (1980) 43–71, doi:10.1002/polc.5070670105.
- [14] V. Percec, Microstructure of polyphenylacetylene obtained by  $\text{MoCl}_5$  and  $\text{WCl}_6$  type catalysts, *Polym. Bull.* 10 (1983) 1–7, doi:10.1007/BF00263230.
- [15] J. Kunzler, V. Percec, Living polymerization of aryl substituted acetylenes by  $\text{MoCl}_5$  and  $\text{WCl}_6$  based initiators: the ortho phenyl substituent effect, *J. Polym. Sci. Part A: Polym. Chem.* 28 (1990) 1221–1236, doi:10.1002/pola.1990.080280522.
- [16] S. Chandrasekhar, B.K. Sadashiva, K.A. Suresh, Liquid crystals of disc-like molecules, *Pramana - J Phys* 9 (1977) 471–480, doi:10.1007/BF02846252.
- [17] V. Percec, D. Sahoo, Discotic liquid crystals 45 years later. Dendronized discs and crowns increase liquid crystal complexity to columnar from spheres, cubic Frank-Kasper, liquid quasicrystals and memory-effect induced columnar bundles, *Giant* 12 (2022) 100127, doi:10.1016/j.giant.2022.100127.
- [18] E. Fontes, P.A. Heiney, d.J. WH, Liquid-crystalline and helical order in a discotic mesophase, *Phys. Rev. Lett.* 61 (1988) 1202–1205, doi:10.1103/PhysRevLett.61.1202.
- [19] E. Fontes, P.A. Heiney, Molecular disorder in columnar-phase of discotic liquid-crystal strands, *Phys. Rev. A.* 37 (1988) 1329–1334, doi:10.1103/PhysRevA.37.1329.
- [20] D. Adam, P. Schuhmacher, J. Simmerer, L. Häussling, K. Siemersmeyer, K.H. Etzbach, H. Ringsdorf, D. Haarer, Fast photoconduction in the highly ordered columnar phase of a discotic liquid crystal, *Nature* 371 (1994) 141–143, doi:10.1038/371141a0.
- [21] J. Billard, J.C. Dubois, N.H. Tinh, A. Zann, Mesophase of disc-like molecules, *Nouv. J. Chim.* 2 (1978) 535–540.
- [22] N.H. Tinh, C. Destrade, H. Gasparoux Destrade, Nematic disc-like liquid crystals, *Phys. Lett. A* 72A (1979) 251–254, doi:10.1016/0375-9601(79)90019-7.
- [23] A.M. Levelut, Structure of a disk-like mesophase, *J. Phys. Lett.* 40 (1979) L81–L84, doi:10.1051/jphyslet:0197900400408100.
- [24] M. Cotrait, P. Marsau, C. Destrade, J. Malthête, Crystalline arrangement of some disc like compounds, *J. Phys.* 40 (1979) L519–L522, doi:10.1051/jphyslet:019790040019051900.jpa-00231678.
- [25] A.M. Levelut, Structures of mesophases of disc-like molecules, *J. Chim. Phys.* 80 (1983) 149–161, doi:10.1051/jcp.1983800149.
- [26] A.M. Levelut, P. Oswald, A. Ghanem, Structure of the 2 columnar phases of a chiral triphenylene ester, 45 (1984) 745–754, doi:10.1051/jphys:01984004504074500.
- [27] R.J. Bushby, O.R. Lozman, Discotic liquid crystals 25 years on, *Curr. Opin. Coll. Interf. Sci.* 7 (2002) 343–354, doi:10.1016/S1359-0294(02)00085-7.
- [28] J. Malthête, A. Collet, Liquid crystals with a cone-shaped cyclotriphénylene core, *Nouv. J. Chim.* 9 (1985) 151–153.
- [29] H. Zimmermann, R. Poupko, Z. Luz, J. Billard, Pyramidal mesophases, *Z. Naturforsch* (1985) 149–160, doi:10.1515/zna-1985-020840a.
- [30] H. Zimmermann, R. Poupko, Z. Luz, J. Billard, Temperature dependent sign reversal of the optical anisotropy in pyramidal mesophases, *Z. Naturforsch* 41 (1986) 1137–1140, doi:10.1515/zna-1986-0908.
- [31] Z. Luz, R. Poupko, E.J. Wachtela, H. Zimmermann, Mesomorphic properties of the neat enantiomers of a chiral pyramidal liquid crystal, *Phys. Chem. Chem. Phys.* 11 (2009) 9562–9568, doi:10.1039/B908029P.
- [32] J. Malthête, A. Collet, Inversion of the cyclotriphénylene cone in a columnar mesophase: a potential way to ferroelectric materials, *J. Am. Chem. Soc.* 109 (1987) 7544–7545, doi:10.1021/ja00258a057.
- [33] A.M. Levelut, J. Malthête, A. Collet, X-ray structural study of the mesophases of some cone-shaped molecules, *J. Phys.* 47 (1986) 331–357, doi:10.1051/jphys:01986004702035100.
- [34] V. Percec, A.E. Dulcey, M. Peterca, M. Ilies, S. Nummelin, M.J. Sienkowska, P.A. Heiney, Principles of self-assembly of helical pores from dendritic dipeptides, *Proc. Natl. Acad. Sci. U.S.A.* 103 (2006) 2518–2523, doi:10.1073/pnas.0509676103.
- [35] V. Percec, M.N. Holera, S. Uchida, W.-D. Cho, G. Ungar, Y. Lee, D.J.P. Yeardley, Exploring and expanding the three-dimensional structural diversity of supramolecular dendrimers with the aid of libraries of alkali metals of their AB3 minidendritic carboxylates, *Chem. Eur. J.* 8 (2002) 1106–1117, doi:10.1002/1521-3765(200203018:5(1106:AID-CHEM1106)3.0.CO;2-G.
- [36] V. Percec, M. Glodde, M. Peterca, A. Rapp, I. Schnell, H.W. Spiess, T.K. Bera, Y. Miura, V.S.K. Balagurusamy, E. Aqad, P.A. Heiney, Self-assembly of semifluorinated dendrons attached to electron-donor groups mediates their  $\pi$ -stacking via a helical pyramidal column, *Chem. Eur. J.* 12 (2006) 6298–6314, doi:10.1002/chem.200501195.
- [37] V. Percec, A.E. Dulcey, M. Peterca, M. Ilies, M.J. Sienkowska, P.A. Heiney, Programming the internal structure and stability of helical pores self-assembled from dendritic dipeptides via the protective groups of the peptide, *J. Am. Chem. Soc.* 127 (2005) 17902–17909, doi:10.1021/ja056313h.
- [38] A. Rapp, I. Schnell, D. Sebastiani, S.P. Brown, V. Percec, H.W. Spiess, Supramolecular assembly of dendritic polymers elucidated by  $^1\text{H}$  and  $^{13}\text{C}$  solid-state MAS NMR spectroscopy, *J. Am. Chem. Soc.* 125 (2003) 13284–13297, doi:10.1021/ja035127d.
- [39] V. Percec, T.K. Bera, M. Glodde, Q. Fu, V.S.K. Balagurusamy, P.A. Heiney, Hierarchical self-assembly, coassembly, and self-organization of novel liquid crystalline lattices and superlattices from a twin-tapered dendritic benzamide and its four-cylinder-bundle supramolecular polymer, *Chem. Eur. J.* 9 (2003) 921–935, doi:10.1002/chem.200390114.
- [40] G. Ungar, D. Abramic, V. Percec, J.A. Heck, Self-assembly of twin tapered bisamides into supramolecular columns exhibiting hexagonal columnar mesophases. Structural evidence for a microsegregated model of the supramolecular column, *Liq. Cryst.* 21 (1996) 73–86, doi:10.1080/02678299608033797.

[41] C. Roche, H.-J. Sun, M.E. Prendergast, P. Leowanawat, B.E. Partridge, P.A. Heiney, F. Araoka, R. Graf, H.W. Spiess, X. Zeng, G. Ungar, V. Percec, Homochiral columns constructed by chiral self-sorting during supramolecular helical organization of hat-shaped molecules, *J. Am. Chem. Soc.* 136 (2014) 7169–7185, doi:10.1021/ja5035107.

[42] C. Roche, H.-J. Sun, P. Leowanawat, F. Araoka, B.E. Partridge, M. Peterca, D.A. Wilson, M.E. Prendergast, P.A. Heiney, R. Graf, H.W. Spiess, X. Zeng, G. Ungar, V. Percec, A supramolecular helix that disregards chirality, *Nat. Chem.* 8 (2016) 80–89, doi:10.1038/nchem.2397.

[43] V. Percec, W.-D. Cho, G. Ungar, D.J.P. Yeadley, From molecular flat tapers, discs, and cones to supramolecular cylinders and spheres using Fréchet-type monodendrons modified on their periphery, *Angew. Chem. Int. Ed.* 39 (2000) 1597–1602, doi:10.1002/(SICI)1521-3773(20000502)39:9(1597)::AID-ANIE15973.0.CO;2-1.

[44] V. Percec, A.E. Dulcey, V.S.K. Balagurusamy, Y. Miura, J. Smidrkal, M. Peterca, S. Nummelin, U. Edlund, S.D. Hudson, P.A. Heiney, H. Duan, S.N. Magonov, S.A. Vinogradov, Self-assembly of dendritic dipeptides into helical pores, *Nature* 430 (2004) 764–768, doi:10.1038/nature02770.

[45] B.M. Rosen, C.J. Wilson, D.A. Wilson, M. Peterca, M.R. Imam, V. Percec, Dendron-mediated self-assembly, disassembly, and self-organization of complex systems, *Chem. Rev.* 109 (2009) 6275–6540, doi:10.1021/cr900157q.

[46] S.D. Hudson, H.-T. Jung, V. Percec, W.-D. Cho, G. Johansson, G. Ungar, V.S.K. Balagurusamy, Direct visualization of individual cylindrical and spherical supramolecular dendrimers, *Science* 278 (1997) 449–452, doi:10.1126/science.278.5337.449.

[47] V. Percec, W.-D. Cho, G. Ungar, D.J.P. Yeadley, Synthesis and structural analysis of two constitutional isomeric libraries of AB<sub>2</sub>-based monodendrons and supramolecular dendrimers, *J. Am. Chem. Soc.* 123 (2001) 1302–1315, doi:10.1021/ja0037771.

[48] V. Percec, W.-D. Cho, P.E. Mosier, G. Ungar, D.J.P. Yeadley, Structural analysis of cylindrical and spherical supramolecular dendrimers quantifies the concept of monodendron shape control by generation number, *J. Am. Chem. Soc.* 120 (1998) 11061–11070, doi:10.1021/ja0019007.

[49] V. Percec, G. Johansson, J. Heck, G. Ungar, S.V. Batty, Molecular recognition directed self-assembly of supramolecular cylindrical channel-like architectures from 6,7,9,10,12,13,15,16-octahydro-1,4,7,10,13-pentaoxabenzocyclopentadecen-2-ylmethyl 3,4,5-tris(p-dodecyloxybenzoyloxy)benzoate, *J. Chem. Soc., Perkin Trans. 1* (1993) 1411–1420, doi:10.1039/P19930001411.

[50] H.-J. Sun, S. Zhang, V. Percec, From structure to function via complex supramolecular dendrimer systems, *Chem. Soc. Rev.* 44 (2015) 3900–3923, doi:10.1039/C4CS00249K.

[51] V. Percec, C.-H. Ahn, T.K. Bera, G. Ungar, D.J.P. Yeadley, Coassembly of a hexagonal columnar liquid crystalline superlattice from polymer(s) coated with a three-cylindrical bundle supramolecular dendrimer, *Chem. Eur. J.* 5 (1999) 1070–1083, doi:10.1002/(SICI)1521-3765(19990301)5:3(1070)::AID-CHEM10703.0.CO;2-9.

[52] V. Percec, M.R. Imam, T.K. Bera, V.S.K. Balagurusamy, M. Peterca, P.A. Heiney, Self-assembly of semifluorinated Janus-dendritic benzamides into bilayered pyramidal columns, *Angew. Chem. Int. Ed.* 44 (2005) 4739–4745, doi:10.1002/anie.200501254.

[53] V. Percec, M.R. Imam, M. Peterca, D.A. Wilson, R. Graf, H.W. Spiess, V.S.K. Balagurusamy, P.A. Heiney, Self-assembly of dendronized triphenylenes into helical pyramidal columns and chiral spheres, *J. Am. Chem. Soc.* 131 (2009) 7662–7677, doi:10.1021/ja8094944.

[54] V. Percec, M. Peterca, M.J. Sienkowska, M.A. Ilies, E. Aqad, J. Smidrkal, P.A. Heiney, Synthesis and retrostructural analysis of libraries of AB<sub>3</sub> and constitutional isomeric AB<sub>2</sub> phenylpropyl ether-based supramolecular dendrimers, *J. Am. Chem. Soc.* 128 (2006) 3324–3334, doi:10.1021/ja060062a.

[55] B.M. Rosen, D.A. Wilson, C.J. Wilson, M. Peterca, B.C. Won, C. Huang, L.R. Lipski, X. Zeng, G. Ungar, P.A. Heiney, V. Percec, Predicting the structure of supramolecular dendrimers via the analysis of libraries of AB<sub>3</sub> and constitutional isomeric AB<sub>2</sub> biphenylpropyl ether self-assembling dendrons, *J. Am. Chem. Soc.* 131 (2009) 17500–17521, doi:10.1021/ja907882n.

[56] V. Percec, B.C. Won, M. Peterca, P.A. Heiney, Expanding the structural diversity of self-assembling dendrons and supramolecular dendrimers via complex building blocks, *J. Am. Chem. Soc.* 129 (2007) 11265–11278, doi:10.1021/ja073714j.

[57] M.S. Kaucher, M. Peterca, A.E. Dulcey, A.J. Kim, S.A. Vinogradov, D.A. Hammer, P.A. Heiney, V. Percec, Selective transport of water mediated by porous dendritic dipeptides, *J. Am. Chem. Soc.* 129 (2007) 11698–11699, doi:10.1021/ja076066c.

[58] V. Percec, J. Heck, M. Lee, G. Ungar, A. Alvarez-Castillo, Poly[2-vinyloxyethyl 3,4,5-tris[4-(n-dodecanyoxy)benzoyl]benzoate]: a self-assembled supramolecular polymer similar to tobacco mosaic virus, *J. Mater. Chem.* 2 (1992) 1033–1039, doi:10.1039/JM9920201033.

[59] V. Percec, M.R. Imam, M. Peterca, P. Leowanawat, Self-organizable vesicular columns assembled from polymers dendronized with semifluorinated Janus dendrimers act as reverse thermal actuators, *J. Am. Chem. Soc.* 134 (2012) 4408–4420, doi:10.1021/ja2118267.

[60] V. Percec, J.A. Heck, D. Tomazos, G. Ungar, The influence of the complexation of sodium and lithium triflate on the self-assembly of tubular-supramolecular architectures displaying a columnar mesophase based on taper-shaped monoesters of oligoethylene oxide with 3,4,5-tris(p-(n-dodecan-1-yloxy)benzoyl)benzoic acid and of their polymethacrylates, *J. Chem. Soc., Perkin Trans. 2* (1993) 2381–2388, doi:10.1039/P29930002381.

[61] Y.K. Kwon, S. Chvalun, A.-I. Schneider, J. Blackwell, V. Percec, J.A. Heck, Supramolecular tubular structures of a polymethacrylate with tapered side groups in aligned hexagonal phases, *Macromolecules* 27 (1994) 6129–6132, doi:10.1021/ma00099a029.

[62] V. Percec, D. Schlueter, Mechanistic investigations on the formation of supramolecular cylindrical shaped oligomers and polymers by living ring opening metathesis polymerization of a 7-oxanorbornene monomer substituted with two tapered monodendrons, *Macromolecules* 30 (1997) 5783–5790, doi:10.1021/ma970157k.

[63] Y.K. Kwon, S.N. Chvalun, J. Blackwell, V. Percec, J.A. Heck, Effect of temperature on the supramolecular tubular structure in oriented fibers of a poly(methacrylate) with tapered side groups, *Macromolecules* 28 (1995) 1552–1558, doi:10.1021/ma00109a029.

[64] V. Percec, D. Schlueter, J.C. Ronda, G. Johansson, G. Ungar, J.P. Zhou, Tubular architectures from polymers with tapered side groups. Assembly of side groups via a rigid helical chain conformation and flexible helical chain conformation induced via assembly of side groups, *Macromolecules* 29 (1996) 1464–1472, doi:10.1021/ma951244k.

[65] V. Percec, D. Schlueter, Y.K. Kwon, J. Blackwell, M. Moeller, P.J. Slangen, Dramatic stabilization of a hexagonal columnar mesophase generated from supramolecular and macromolecular columns by the semifluorination of the alkyl groups of their tapered building blocks, *Macromolecules* 28 (1995) 8807–8818, doi:10.1021/ma00130a013.

[66] G. Johansson, V. Percec, G. Ungar, D. Abramic, Molecular recognition directed self-assembly of tubular liquid crystalline and crystalline supramolecular architectures from taper shaped (15-crown-5)methyl 3,4,5-tris(p-alkoxybenzoyloxy)benzoates and (15-crown-5)methyl 3,4,5-tris(p-dodecyloxybenzoyloxy)benzoate, *J. Chem. Soc., Perkin Trans. 1* (1994) 447–459, doi:10.1039/P19940000447.

[67] V. Percec, D. Schlueter, G. Ungar, S.Z.D. Cheng, A. Zhang, Hierarchical control of internal superstructure, diameter, and stability of supramolecular and macromolecular columns generated from tapered monodendritic building blocks, *Macromolecules* 31 (1998) 1745–1762, doi:10.1021/ma971459p.

[68] V. Percec, D. Tomazos, J. Heck, H. Blackwell, G. Ungar, Self-assembly of taper-shaped monoesters of oligo(ethylene oxide) with 3,4,5-tris(n-dodecan-1-yloxy)benzoic acid and of their polymethacrylates into tubular supramolecular architectures displaying a columnar hexagonal mesophase, *J. Chem. Soc., Perkin Trans. 2* (1994) 31–44, doi:10.1039/P29940000031.

[69] V. Percec, M. Glodde, G. Johansson, V.S.K. Balagurusamy, P.A. Heiney, Transformation of a spherical supramolecular dendrimer into a pyramidal columnar supramolecular dendrimer mediated by the fluorophobic effect, *Angew. Chem. Int. Ed.* 42 (2003) 4338–4342, doi:10.1002/anie.200351804.

[70] M. Peterca, V. Percec, M.R. Imam, P. Leowanawat, K. Morimitsu, Molecular structure of helical supramolecular dendrimers, *J. Am. Chem. Soc.* 130 (2008) 14840–14852, doi:10.1021/ja806524m.

[71] G. Ungar, V. Percec, M.N. Holerca, G. Johansson, J.A. Heck, Heat-shrinking spherical and columnar supramolecular dendrimers: Their interconversion and dependence of their shape on molecular taper angle, *Chem. Eur. J.* 6 (2000) 1258–1266, doi:10.1002/(SICI)1521-3765(20000403)6:7(1258)::AID-CHEM12583.0.CO;2-O.

[72] V. Percec, C.-H. Ahn, G. Ungar, D.J.P. Yeadley, M. Möller, S.S. Sheiko, Controlling polymer shape through the self-assembly of dendritic side-groups, *Nature* 391 (1998) 161–164, doi:10.1038/34384.

[73] V. Percec, M. Glodde, T.K. Bera, Y. Miura, I. Shiyanskaya, K.D. Singer, V.S.K. Balagurusamy, P.A. Heiney, I. Schnell, A. Rapp, H.-W. Spiess, S.D. Hudson, H. Duan, Self-organization of supramolecular helical dendrimers into complex electronic materials, *Nature* 419 (2002) 384–387, doi:10.1038/nature01072.

[74] J.G. Rudick, V. Percec, Induced Helical Backbone conformations of self-organizable dendronized polymers, *Acc. Chem. Res.* 41 (2008) 1641–1652, doi:10.1021/ar080086w.

[75] V. Percec, C.-H. Ahn, W.-D. Cho, A.M. Jamieson, J. Kim, T. Leman, M. Schmidt, M. Gerle, M. Möller, S.A. Prokhorova, S.S. Sheiko, S.Z.D. Cheng, A. Zhang, G. Ungar, D.J.P. Yeadley, Visualizable cylindrical macromolecules with controlled stiffness from backbones containing libraries of self-assembling dendritic side groups, *J. Am. Chem. Soc.* 120 (1998) 8619–8631, doi:10.1021/ja981211v.

[76] V. Percec, J.G. Rudick, M. Peterca, M. Wagner, M. Obata, C.M. Mitchell, W.-D. Cho, V.S.K. Balagurusamy, P.A. Heiney, Thermoreversible cis–cisoidal to cis–transoidal isomerization of helical dendronized polyphenylacetylenes, *J. Am. Chem. Soc.* 127 (2005) 15257–15264, doi:10.1021/ja055406w.

[77] V. Percec, J.G. Rudick, M. Peterca, P.A. Heiney, Nanomechanical function from self-organizable dendronized helical polyphenylacetylenes, *J. Am. Chem. Soc.* 130 (2008) 7503–7508, doi:10.1021/ja801863e.

[78] V. Percec, C.M. Mitchell, W.-D. Cho, S. Uchida, M. Glodde, G. Ungar, X. Zeng, Y. Liu, V.S.K. Balagurusamy, P.A. Heiney, Designing libraries of first generation AB3 and AB2 self-assembling dendrons via the primary structure generated from combinations of (AB)<sub>n</sub>–AB3 and (AB)<sub>n</sub>–AB2 building blocks, *J. Am. Chem. Soc.* 126 (2004) 6078–6094, doi:10.1021/ja049846j.

[79] V. Percec, M. Obata, J.G. Rudick, B.B. De, M. Glodde, T.K. Bera, S.N. Magonov, V.S.K. Balagurusamy, P.A. Heiney, Synthesis, structural analysis, and visualization of poly(2-Ethynyl-9-substituted carbazole)s and poly(2-Ethynyl-9-substituted carbazole)s containing chiral and achiral minidendritic substituents, *J. Polym. Sci. Part A: Polym. Chem.* 40 (2002) 3509–3533, doi:10.1002/pola.10458.

[80] V. Percec, J. Heck, D. Tomazos, F. Falkenberg, H. Blackwell, G. Ungar, Self-assembly of taper-shaped monoesters of oligo(ethylene oxide) with 3,4,5-tris(p-dodecyloxybenzoyloxy)benzoic acid and of their polymethacrylates into tubular supramolecular architectures displaying a columnar mesophase, *J. Chem. Soc., Perkin Trans. 1* (1993) 2799–2811, doi:10.1039/P19930002799.

[81] V. Percec, W.-D. Cho, G. Ungar, Increasing the diameter of cylindrical and spherical supramolecular dendrimers by decreasing the solid angle of their monodendrons via periphery functionalization, *J. Am. Chem. Soc.* 122 (2000) 10273–10281, doi:10.1021/ja0024643.

[82] V. Percec, E. Aqad, M. Peterca, J.G. Rudick, L. Lemon, J.C. Ronda, B.B. De, P.A. Heiney, E.W. Meijer, Steric communication of chiral information observed in dendronized polyacetylenes, *J. Am. Chem. Soc.* 128 (2006) 16365–16372, doi:10.1021/ja0665848.

[83] V. Percec, H.-J. Sun, P. Leowanawat, M. Peterca, R. Graf, H.W. Spiess, X. Zeng, G. Ungar, P.A. Heiney, Transformation from kinetically into thermodynamically controlled self-organization of complex helical columns with 3D periodicity assembled from dendronized perylene bisimides, *J. Am. Chem. Soc.* 135 (2013) 4129–4148, doi:10.1021/ja400639q.

[84] P.A. Heiney, Commission on powder diffraction newsletter, 32 (2005) 9–11.

[85] N. Boden, R.C. Borner, R.J. Bushby, A.N. Cammidge, M.V. Jesudason, The synthesis of triphenylene-based discotic mesogens New and improved routes, *Liq. Cryst.* 15 (1993) 851–858, doi:10.1080/02678299308036504.

[86] N. Boden, R.J. Bushby, A.N. Cammidge, A quick-and-easy route to unsymmetrically substituted derivatives of triphenylene: preparation of polymeric discotic liquid crystals, *J. Chem. Soc., Chem. Commun.* (1994) 465–466, doi:10.1039/C39940000465.

[87] F.C. Krebs, N.C. Schiott, W. Batsberg, K. Bechgaard, Purification of 2,3,6,7,10,11-hexamethoxytriphenylene and preparation of hexakis carbonylmethyl and hexakis cyanomethyl derivatives of 2,3,6,7,10,11-hexahydroxytriphenylene, *Synthesis* 11 (1997) 1285–1290, doi:10.1055/s-1997-3188.

[88] E.O. Arikainen, N. Boden, R.J. Bushby, J. Clements, B. Movaghari, A. Wood, Effects of side-chain length on the charge transport properties of discotic liquid crystals and their implications for the transport mechanism, *J. Mater. Chem. 5* (1995) 2161–2165, doi:10.1039/JM9950502161.

[89] N. Spielberg, M. Sarkar, Z. Luz, R. Poupko, J. Billard, H. Zimmermann, The discotic mesophases of octaalkyloxy- and octaalkanoyloxyorthocyclophanes, *Liq. Cryst.* 15 (1993) 311–330, doi:10.1080/02678299308029134.

[90] V. Percec, C.G. Cho, C. Pugh, Alkyloxy-substituted CTTV derivatives that exhibit columnar mesophases, *J. Mater. Chem.* 1 (1991) 217–222, doi:10.1039/JM9910100217.

[91] J.D. Watson, E.H.C. Crick, Molecular structure of nucleic acids: a structure for deoxyribose nucleic acid, *Nature* 171 (1953) 737–738, doi:10.1038/171737a0.

[92] B.E. Partridge, L. Wang, D. Sahoo, J.T. Olsen, P. Leowanawat, C. Roche, H. Ferreira, K.J. Reilly, X. Zeng, G. Ungar, P.A. Heiney, R. Graf, H.W. Spiess, V. Percec, Sequence-defined dendrons dictate supramolecular cogwheel assembly of dendronized perylene bisimides, *J. Am. Chem. Soc.* 141 (2019) 15761–15766, doi:10.1021/jacs.9b08714.

[93] L. Wang, B.E. Partridge, N. Huang, J.T. Olsen, D. Sahoo, X. Zeng, G. Ungar, R. Graf, H.W. Spiess, V. Percec, Extraordinary acceleration of cogwheel helical self-organization of dendronized perylene bisimides by the dendron sequence encoding their tertiary structure, *J. Am. Chem. Soc.* 142 (2020) 9525–9536, doi:10.1021/jacs.0c03353.

[94] M.N. Holerca, D. Sahoo, B.E. Partridge, M. Peterca, X. Zeng, G. Ungar, V. Percec, Dendronized poly(2-oxazoline) displays within only five monomer repeat units liquid quasicrystal, A15 and  $\sigma$  Frank-Kasper phases, *J. Am. Chem. Soc.* 140 (2018) 16941–16947, doi:10.1021/jacs.8b11103.

[95] K.A. Andreopoulou, M. Peterca, D.A. Wilson, B.E. Partridge, P.A. Heiney, V. Percec, Demonstrating the  $\delta_1$ -helicity and nanomechanical function of self-organizable dendronized polymethacrylates and polyacrylates, *Macromolecules* 50 (2017) 5271–5284, doi:10.1021/acs.macromol.7b01216.

[96] M.N. Holerca, D. Sahoo, M. Peterca, B.E. Partridge, P.A. Heiney, V. Percec, A tetragonal phase self-organized from unimolecular spheres assembled from a substituted poly(2-oxazoline), *Macromolecules* 50 (2017) 375–385, doi:10.1021/acs.macromol.6b02298.

[97] V. Percec, C.G. Cho, C. Pugh, D. Tomazos, Synthesis and characterization of branched liquid-crystalline polyethers containing cyclotetraveratrylene-based disk-like mesogens, *Macromolecules* 25 (1992) 1164–1176, doi:10.1021/ma00029a025.

[98] Y. Snir, R.D. Kamien, Entropically driven helix formation, *Science* 307 (2005) 1067, doi:10.1126/science.11062.

[99] D. Chakrabarti, S.N. Fejer, D.J. Wales Rational design of helical architectures, in: *Proc. Natl. Acad. Sci. U.S.A.*, 106, 2009, pp. 20164–20167, doi:10.1073/pnas.0906676106.

[100] M. Peterca, M.R. Imam, S.D. Hudson, B.E. Partridge, D. Sahoo, P.A. Heiney, M.L. Klein, V. Percec, Complex arrangement of orthogonal nanoscale columns via a supramolecular orientational memory effect, *ACS Nano* 10 (2016) 10480–10488, doi:10.1021/acsnano.6b06419.

[101] D. Sahoo, M. Peterca, E. Aqad, B.E. Partridge, P.A. Heiney, R. Graf, H.W. Spiess, X. Zeng, V. Percec, Tetrahedral arrangements of perylene bisimide columns via supramolecular orientational memory, *ACS Nano* 11 (2017) 983–991, doi:10.1021/acsnano.6b07599.

[102] N. Huang, M.R. Imam, M.J. Sienkowska, M. Peterca, M.N. Holerca, D.A. Wilson, B.M. Rosen, B.E. Partridge, Q. Xiao, V. Percec, Supramolecular spheres assembled from covalent and supramolecular dendritic crowns dictate the supramolecular orientational memory effect mediated by Frank-Kasper phases, *Giant* 1 (2020) 100001, doi:10.1016/j.giant.2020.100001.

[103] N. Huang, Q. Xiao, M. Peterca, X. Zeng, V. Percec, Self-organisation of rhombitruncated cuboctahedral hexagonal columns from an amphiphilic Janus dendrimer, *Molecular Physics* 119 (2021) 19–20, doi:10.1080/00268976.2021.1902586.

[104] V. Percec, N. Huang, Q. Xiao, B.E. Partridge, D. Sahoo, M.R. Imam, M. Peterca, R. Graf, H.-W. Spiess, X. Zeng, G. Ungar, Self-organization of rectangular bipyramidal helical columns by supramolecular orientational memory epitaxially nucleated from a Frank-Kasper  $\sigma$  phase, *Giant* 9 (2022) 100084, doi:10.1016/j.giant.2021.100084.

[105] V. Percec, S. Wang, N. Huang, B.E. Partridge, X. Wang, D. Sahoo, D.J. Hoffman, J. Malineni, M. Peterca, R.L. Jezorek, N. Zhang, H. Daud, P.D. Sung, E.R. McClure, S.L. Song, An accelerated modular-orthogonal Ni-catalyzed methodology to symmetric and nonsymmetric constitutional isomeric AB<sub>2</sub> to AB<sub>9</sub> dendrons exhibiting unprecedented self-organizing principles, *J. Am. Chem. Soc.* 143 (2021) 17724–17743, doi:10.1021/jacs.1c08502.

[106] D. Sahoo, M. Peterca, M.R. Imam, B.E. Partridge, Q. Xiao, V. Percec, Conformationally flexible dendronized cyclotetraveratrylenes (CTTVs) self-organize a large diversity of chiral columnar, Frank-Kasper and quasicrystal phases, *Giant* 10 (2022) 100096, doi:10.1016/j.giant.2022.100096.

[107] M.R. Imam, M. Peterca, Q. Xiao, V. Percec, Enhancing conformational flexibility of dendronized triphenylene via diethylene glycol linkers lowers transitions of helical columnar, Frank-Kasper, and quasicrystal phases, *Giant* 10 (2022) 100098, doi:10.1016/j.giant.2022.100098.

[108] M. Peterca, D. Sahoo, M.R. Imam, Q. Xiao, V. Percec, Searching for the simplest self-assembling dendron to study helical self-organization and supramolecular polymerization, *Giant* 12 (2022) 100118, doi:10.1016/j.giant.2022.100118.

[109] Q. Xiao, N. Rivera-Martinez, C.J. Raab, J.G. Bermudez, M.C. Good, M.L. Klein, V. Percec, Co-assembly of liposomes, dendrimersomes, and polymersomes with amphiphilic Janus dendrimers conjugated to mono- and tris-nitrilotriacetic acid (NTA, TrisNTA) enhances protein recruitment, *Giant* 9 (2022) 100089, doi:10.1016/j.giant.2021.100089.

[110] V. Percec, Q. Xiao, From organic chemistry to chemical biology via macromolecules with Hermann Staudinger, *Giant* 4 (2020) 100036, doi:10.1016/j.giant.2020.100036.

[111] M. Peterca, M.R. Imam, A.E. Dulcey, K. Morimitsu, Q. Xiao, D.S. Maurya, V. Percec, Molecular parameters including fluorination program order during hierarchical helical self-organization of self-assembling dendrons, *Giant* 11 (2022) 100103, doi:10.1016/j.giant.2022.100103.

[112] V. Percec, M.R. Imam, M. Peterca, D.A. Wilson, P.A. Heiney, Self-assembly of dendritic crowns into chiral supramolecular spheres, *J. Am. Chem. Soc.* 131 (2009) 1294–1304, doi:10.1021/ja808778.